JOURNAL OF MATERIALS SCIENCE **37** (2002) 2171 – 2202

Review
Progress in Ostwald ripening theories and their applications to nickel-base superalloys
Part I: *Ostwald ripening theories*

A. BALDAN
Department of Metallurgical and Materials Engineering, Mersin University, Ciftlikkoy, Mersin, Turkey
E-mail: abaldan@mersin.edu.tr

The physical basis behind the Ostwald ripening process for two-phase mixture has been reviewed in detail, using the various theories developed to describe this process. The Ostwald ripening, also termed second phase coarsening, is generally thought to be slow, diffusion-controlled process which occurs subsequent to phase separation under extremely small under-saturation levels. The major advance for the description of this process was made when Lifshitz, Slyozov and Wagner (also known as the LSW theory) published their papers more than fourty years ago. This classical LSW theory predicts that the ripening kinetics and the particle size distribution function are applicable to dilute systems only [i.e. when the volume fraction (Q) of second phase approaces zero: $Q \rightarrow 0$], in which particle-particle interactions are not important. After the publication of the LSW theory, many experimentalists tested the veracity of the theory. Experimentalists have confirmed the prediction of self-similar ripening behavior at long times. However, virtually none of the reported distributions are of the form predicted by the LSW theory. The reported distributions are generally broader and more symmetric than the LSW predictions. It was later realized that a major problem with the LSW approach was the mean field nature of the kinetic equation. In order to remove the zero volume fraction assumption of the LSW theory, the many theories have been developed based on the statistically averaged diffusion interaction of a particle of given size class with its surroundings, using both analytic and numerical methods. Many attempts to determine the statistically averaged growth rate of a particle either do not account for the long-range nature of the diffusional field surrounding the particle, and/or employed *ad hoc* assumptions in an attempt to account for the diffusional interactions between particles. The strength of the diffusional interactions between particles stems from the long range Coulombic nature of the diffusion field surrounding a particle. As a result, particle interactions occur at distances of many particle diameters and restrict the validity of LSW theory to the unrealistic limit of zero volume fraction of coarsening phase. More realistic models of the ripening process at finite-volume fractions (Q) of coarsening phase have been proposed by various workers such as Brailsford-Wynblatt (1979), Voorhees-Glicksman (1983), Marqusee-Rose (1984), Tokuyama-Kawasaki (1984), Enomoto-Tokuyama-Kawasaki (ETK) (1986), and Yao-Elder-Guo-Grant (YEGG) (1993) models. Although a great deal of progress has been made in understanding Ostwald ripening, a fully satisfactory approach has not yet been found, and it has remained a vexing problem in the field. At present, it is very difficult to determine which of these theories best describes coarsening at finite volume fraction. The statistical mechanical theories, developed to describe systems in which $Q \ll 1$, employed the same microscopic equation to describe the coarsening rates of individual particles, but different techniques to perform the statistical averaging. In addition, these theories can be distinguished on yet a finer scale. All of the theories predict that the rate constant will vary as $Q^{1/2}$ in this low volume fraction limit. These theories predict that the scaled time-independent particle radius distributions become broader and more symmetric than those predicted by LSW as the volume fraction increases. Clearly more experimental and theoretical work is necessary in order to settle the subtle disagreement now existing between the various Ostwald ripening theories.

1. Introduction

Coarsening is phase transformation process which has been observed in a large number of metallic and nonmetallic systems where particles with various sizes are dispersed in a matrix. The driving force of this process is the decrease in total surface free energy. The process occurs by the growth of large particles at the expense of smaller ones which dissolve. At any stage during coarsening there is a so-called critical particle radius R^* being in equilibrium with the mean matrix composition; particles with $R > R^*$ will grow and particles with $R < R^*$ will shrink.

Precipitation processes occur by the nucleation and growth of the second phase from a supersaturated solution. The end point is a dispersion of precipitate particles embedded in the matrix, whose sizes vary depending on the nucleation rate (and its time dependence) of the precipitate. Thermodynamically, this state does not satisfy the requirement of a minimum energy configuration because of the excess surface energy represented by the particulate ensemble. The system therefore continues to evolve to the state where the surface energy is lowered as much as possible. In a finite system, the theoretical endpoint of this evolution would be a single precipitate particle that contains the entire volume fraction of the second phase. This evolution of the particle size distribution that is driven by excess surface energy is defined as coarsening.

In general, any first-order transformation process results in a two-phase mixture composed of a dispersed second phase in a matrix. However, as a result of the large surface area present, the mixture is not initially in thermodynamic equilibrium. The total energy of the two-phase system can be decreased via an increase in the size scale of the second phase and thus a decrease in total interfacial area. Such a process is termed *Ostwald ripening or coarsening*, after the physical chemist W. Ostwald, who originally described the process qualitatively [1, 2]. Since the excess energy associated with the total surface area is usually small, such surface energy driven morphological changes typically manifest themselves as the last stage of a first-order phase transformation process. Early attempts by Greenwood [3] and Asimov [4] to construct a quantitative theory of the Ostwald ripening process did not meet with success since both theories are based upon an unrealistic solution for the diffusion field in the matrix. Phase-separation processes frequently result in a polydisperse mixture of two phases of nearly equilibrium compositions and volume fractions. Such mixtures can also be created artificially by irradiating materials to creat voids or, as is done in liquid phase sintering processes, by mixing together powders of different composition. Despites the nearly equilibrium state of the two-phase system, the mixture is not in its lowest energy state. This is because of the polydisperse nature of the mixture itself and the presence of a nonzero interfacial energy. Thus in the absence of elastic stress, the total interfacial area of the system must decrease with time in order for the system to reach thermodynamic equilibrium. There are many ways the system can reduce this excess interfacial area. The process of interest here is when the interfacial area is reduced via a diffusional mass transfer process from regions of high interfacial curvature to regions of low interfacial curvature. As mentioned above, this interfacial area reduction process is called the Ostwald ripening or coarsening. This interfacial energy driven mass transfer process can significantly alter the morphology of the two-phase mixture. In general, the average size-scale of the mixture must increase with time and the number of second phase particles, must decrease with time. This change in the morphology occurs as a result of small particles dissolving and transferring their mass to the larger particles.

A major advance in the theory of Ostwald ripening was made in a paper by Lifshitz and Slyozof [5, 6] and followed by a related paper by Wagner [7] (LSW). In contrast to previous theories, The LSW developed a method for treating an ensemble of dilute coarsening particles, and were able to make quantitative predictions on the long-time behavior of coarsening systems without recourse to a numerical solution of the relevant equations. The limitation of infinite dilution allows the overall kinetic behavior of a such coarsening system to be determined without recourse to the details of the interparticle diffusion field. To treat the continuum problem, LSW made the critical assumption that a particle's coarsening rate is independent of its surroundings. This is tantamount to a "mean field" description of a particle's growth rate. LSW used the hydrodynamic continuity equation describing the particle radii distribution, and were able to derive the well-known results that (a) at long times the cube of the average particle radius should vary linearly with time, (b) that an arbitrary distribution of particle radii when scaled by the average radius should assume a specific time-independent form. Since the time-independent radii distribution predicted by LSW is usually not observed experimentally, it is clear that modifications of the LSW theory are necessary. As a result of the deficiencies in the LSW treatment, many theories of Ostwald ripening are developed based on multi-particle diffusion (MPD) solution. These modern theories (see for example, [8–18]) describing ripening in systems with a finite volume fraction of precipitate particles will be the major part of this paper.

2. Basic equations

Many two-phase mixtures undergo Ostwald ripening, or coarsening, and it is widely held that Ostwald ripening plays a major role in determining the morphology of finely divided two-phase systems. It is also well known that if the rate of second-phase growth or dissolution is not controlled by an interfacial reaction, then the morphological changes occur via the flow of heat or solute to and flow regions of varying interfacial curvature (or chemical potential). Although the fundamental mechanisms responsible for Ostwald ripening are established it has been difficult to construct a realistic theoretical description of the kinetics of coarsening. The major difficulty in developing a description of coarsening is that a solution to the diffusion equation during ripening has not been available in a form which is amenable to

practical systems comprised of a myriad of randomly positioned second-phase regions.

2.1. Thermodynamic driving force for ripening

Competitive growth takes place among precipitates when particles with various sizes are dispersed in a matrix. The growth originates from the concentration gradients around the particles caused by the thermodynamic demand, i.e. the Gibbs-Thomson equation: the concentration at the surface of particles in equilibrium with larger particles is lower than that with smaller particles. Solute atoms flow through the concentration gradients both from the surface of the smaller particles to matrix and from the matrix to the surface of larger particles. During this process, average radius of the particles increases. The phenomena can take place in any stage of precipitation.

Any system of disperse particles statistically distributed in a medium and possessing certain solubility in it will be thermodynamically unstable due to a large interface area. Its decrease in approaching equilibrium is accompanied by particle coarsening whose solubility depends on their radii and is described by the well known Gibbs-Thomson relation

$$C_r = C_e \exp\left[\frac{2\gamma\Omega}{R_B T}\cdot\frac{1}{r}\right] \approx C_e\left[1+\frac{2\gamma\Omega}{R_B T}\cdot\frac{1}{r}\right] \quad (1)$$

where C_e is the solute concentration at a plane interface in the matrix in equilibrium with particle of infinite radius, C_r is the solubility at the surface of a spherical particle with radius r, γ is the specific interfacial energy of the matrix-precipitate particle boundary, Ω is the mean atomic (or molar) volume of the particle, R_B is the Universal gas constant [8.314×10^3 J/(K. kmol)] and T is the absolute temperature. The difference between C_r and C_e induces a diffusive flux of atoms from the smaller to the larger particles. Thus the average particle radius increases and the total number of particles decreases with time, as well as the total free surface enthalpy of the system.

The Gibbs-Thomson relationship describes the solubility of particle atoms in the matrix, which is the basic equation which forms the beginning of the analysis.

2.2. Scaling the Ostwald ripening problem

Dimensionless variables will be employed for the remainder of this paper. An appropriate characteristic length for a system which exchanges during coarsening, through which all quantities of length will be scaled, is the capillarity length l_C defined as

$$l_C = \frac{2\gamma\Omega}{R_B T} \quad (2)$$

A dimensionless time t^* may also be defined as

$$t = \left[\frac{DC_e\Omega}{l_C^2}\right]t^* \quad (3)$$

where t is the time, D is the diffusion coefficient.

Finally a dimensionless concentration θ will be defined as

$$\theta = \frac{C - C_\infty}{C_\infty} \quad (4a)$$

$$\theta = \frac{T - T_m}{T_m} \quad (4b)$$

where θ is a dimensionless pressure, temperature T or solute concentration C, etc depending on the problem, C_∞ is the equilibrium concentration of the matrix phase at a flat surface, and T_m is the bulk melting temperature.

2.3. Equations necessary to describe the ripening kinetics of a two-phase system

Theories of particle coarsening must be statistical in nature since experimental data are essentially statistical samples. There are three equations, which arise in the theory and require solution [19].

(a) a *kinetic equation* describing the growth or shrinkage rate of an individual particle of given size,

(b) a *continuity equation* describing the temporal evolution of a particle size distribution function, and

(c) a *mass conservation equation*, which the solutions to the first two must satisfy to be acceptible.

The kinetics of Ostwald ripening processes often are described by relationships between an average length scale of the mixture and a temporal law with a positive exponent. These scaling laws can be derived from an assumption of sell-similarity of the microstructure with time or from a kinetic equation that describes the growth rate of a second-phase particle with respect to another. For example, Lifshitz and Slyozov (LS) [2, 3] use a kinetic equation appropriate for an infinitely dilute array of spherical particles in a stress-free matrix to predict that the average particle radius should increase as $t^{1/3}$ where t is time. The LS theory assumes that the mechanism responsible for the transformation process is the diffusion of mass from regions of high interfacial curvature to regions of low interfacial curvature. Such a morphological evolution process is consistent with a dimunuation of the total interfacial area (and, hence, total interfacial energy with time) and is called Ostwald ripening.

2.3.1. The kinetic equation

The kinetic equation is usually the difficult to determine for it is based upon a solution to a potentially difficult free-boundary problem. The concentration field equation describing mass flow, which must be solved in both phases, is

$$\nabla^2 C = 0 \quad (5)$$

The justification for neglecting the time-dependence of the concentration field lies in the small interfacial velocities, which are present during ripening, along

with the requirement that an accurate description of the diffusion field is necessary for only small distances away from a particle [20].

One set of boundary conditions is the interfacial concentrations in the matrix and precipitate phases at a curved interface. These boundary conditions, the so-called Gibbs-Thomson equations (see Equation 1), reflect the physical process process behind an interfacial energy-driven ripening process. Using the equilibrium conditions given by Gibbs [21], it is possible to show that the compositions of the α phase, C^{α}, and β phase, C^{β}, in an isothermal system at a curved interface are given by [19, 22]

$$C^{\alpha} = C_e^{\alpha} + l_C^{\alpha}\kappa \tag{6a}$$

$$C^{\beta} = C_e^{\alpha} + l_C^{\beta}\kappa \tag{6b}$$

where l_C is the capillary length (see Equation 2) in the designated phase,

$$l_C^{\alpha} = \frac{\Omega^{\beta}\gamma}{\left(C_e^{\beta} - C_e^{\alpha}\right)G_m^{''\alpha}} \tag{7a}$$

$$l_C^{\beta} = \frac{\left[\Omega_1^B\left(1 - C_e^{\alpha}\right) + \Omega_2^{\beta}C_e^{\alpha}\right]\gamma}{\left(C_e^{\beta} - C_e^{\alpha}\right)G_m^{''\beta}} \tag{7b}$$

Ω^{β} is the molar volume of β, Ω_i^{β} is the partial molar volume of component i in the β phase, C_e denotes the equlibrium mole fraction of component 2 at a planar interface in the noted phase, κ is the sum of the principle curvatures of the interface taken positive for a spherical particle β, and $G_m^{''}$ is the second derivative of the molar free energy of the designated phase with respect to composition. These expressions for the equilibrium interfacial concentrations at a curved interface are valid for a general nonideal-nondilute solution, but are limited by the condition $|C(\kappa) - C_e| \leq 1$ in both phases. In addition, they reduce to the more standard forms for the Gibbs-Thomson equations. For example, in a dilute-ideal solution $l_C^{\alpha} = \Omega^{\beta}C_e^{\alpha}/R_BT$. These equations show that the concentration at an interface with high curvature will be above that at an interface with low curvature. In systems with nonzero solute diffusivities, this difference will cause mass to flow from an interface with high curvature to an interface with low curvature, thus resulting in the disappearence of regions of high interfacial curvature.

The other boundary condition is that the composition of the matrix is given by a mean-field value of C_e. Finally, the interfacial velocity is given by the flux conservation condition at the interface [19],

$$(C^{\beta} - C^{\alpha})V_n = (D^{\beta}\nabla C^{\beta} - D^{\alpha}\nabla C^{\alpha}) \cdot n \tag{8}$$

where V_n is the local velocity of the interface in the direction of the interface normal, n is the normal to the interface, which is pointing from α to β, D is the diffusion coefficient in the specified phase, and the concentration gradients are evaluated at the interface in the designated phase.

Although the morphology of the second-phase particles is not specified, it is usually chosen to be spherical.

2.3.2. The continuity equation

If particles flow through particle size space in a continuous manner, the time rate of change of the number of particles per unit volume of size R to $R + \mathrm{d}R$, $f(R, t)$, is given [19] by the flowing continuity equation

$$\frac{\partial f}{\partial t} + \frac{\partial(f\,\mathrm{d}R/\mathrm{d}t)}{\partial R} = 0 \tag{9}$$

where $\mathrm{d}R/\mathrm{d}t$ is the growth or shirinkage rate of a particle as given by the kinetic equation, and t is time. The assumption of a continuous flow of particles specifically exludes any process that would give rise to discontinuous jumps in particle size during the corsening process, such as nucleation or coalescence. The value of the mean-field concentration in the matrix required in the kinetic equation follows from a constraint that the total number of solute in the system must be conserved,

$$C_{\mathrm{o}} = (1 - Q_{\beta})C_{\infty}C^{\beta} \tag{10}$$

where Q_{β} is the mole fraction of β, and C_{o} is the mole fraction of solute in the alloy. The mass conservation condition must be added explicitly, since the time derivation in the diffusion equation has been neglected.

2.3.3. The mass conservation equation

The mass conservation equation implies that if the mean-field condition is a function of time during ripening, then the mole fraction of the second phase particle Q must also be a function of time. The mole fraction, is related to the particle size distribution function $f(R, t)$ as

$$Q = G\int_0^{\infty} R^3 f(R, t)\,\mathrm{d}R \tag{11}$$

where G is a geometrical factor that depends on the particle morphology.

3. Theoretical background in Ostwald ripening theories

Following two main models will be presented before describing the modern Ostwald ripening theories.

(a) one based upon an approximation solution to the *multiparticle diffusion* problem using computer simulation techniques, and

(b) *statistical nonlinear mean-field theory* which is capable of describing coarsening behavior over the wide range of volume fraction of particles encountered in materials.

3.1. Multiparticle diffusion (MDP) problem

Voorhees [23] and Voorhees and Glicksman [24] have described a method for solving the multiparticle

diffusion problem (MDP). They used point-source representation of spherical particles interacting with each other via their diffusion fields [25]. The particles are positioned randomly within a reference unit cell at a specified volume fraction, and periodic boundary conditions are used to fill all space with coarsening particles.

The diffusion field whithin the matrix of a system of coarsening particles in the quasistatic approximation is given by,

$$\nabla^2(\theta) = \sum_{i=1}^{N} -4\pi B_i \delta(r - r_i) \tag{12}$$

where θ is a dimensionless temperature or concentration (see Equation 4) r is a dimensionless vector locating the arbitrary field point, r_i is a dimensionless vector which locates the center of the ith particle, δ is a Dirac delta function, and B_i is a constant whose magnitude is a measure of the strength of the point source ($B_i > 0$) or sink ($B_i < 0$), N is the number of sources or sinks in the system. All quantities which have units of length are scaled by the capillary length l_C (see Equation 2). The solution to Equation 12 is

$$\theta(r) = B_{\mathrm{o}} + \sum \frac{B_i}{|r - r_i|} \tag{13}$$

where B_{o} is a constant. The constants B_{o} and B_i are determined by applying the following boundary conditions:

$$\theta_{\mathrm{AV}}\Big|_{R_i} = -\frac{1}{R_i} \tag{14}$$

and

$$\sum B_i = 0 \tag{15}$$

where $\theta_{\mathrm{AV}}|_{R_i}$ is the surface averaged dimensionless temperature or concentration of the ith particle. Equation 14 states that the surface averaged concentration is to be set equal to the dimensionless temperature or concentration as specified by the Gibbs-Thomson (see Equation 1).

3.2. Mean-field statistical models

In addition to the MDP described in the previous section, Voorhees and Glicksman [24] investigated also the *average* behavior of an ensemble of particles dispersed in a matrix at a specified volume fraction. It is assumed that a typical particle within a size class as though it alone was interacting with the average environment established by all the other particles. The interacting environment is represented by a *mean* potential $\alpha = \rho^{*-1}$, where $\rho^* = R^*/R_{\mathrm{AV}}$ is the ratio of the radius of the critical particle, i.e., the particle for which $\mathrm{d}R/\mathrm{d}t = 0$, to that of the average particle. $R^* = R_{\mathrm{AV}}$ and $\rho^* = 1$ for zero volume fraction. The mean potential α acts at a distance ρ_o from the center of the typical particle of size class $\rho = R/R_{\mathrm{AV}}$. Again, at zero volume fraction $\rho_o = \infty$, so the mean field $\alpha = 1$ is established far from a particle. At finite volume fractions, however, the critical radius is larger than the average radius so α is less than unity. If a stochastic potential is defined as $\phi = -\theta R_{\mathrm{AV}}$, where θ is the dimensionless diffusion potential (Equation 13), and R_{AV} is the dimensionless average particle radius at some instant in time, then the mean-field problem may be specified in the following general form: $\nabla^2\phi(\xi) = 0$, $\rho \le \xi \le \rho_o$, subject to the boundary conditions $\phi = 1/\rho$ at $\xi = r/R_{\mathrm{AV}}$, which is a dimensionless distance r normalized to the time-dependent quantity R_{AV}. The property of $\phi(\xi)$ which is of special value here is termed *scale dilatation invariance.* Scale dilatation invariance implies that the diffusion problem between a typical particle of size class ρ and the mean field are time independent in the variable ξ, despite the fact that R_{AV} is a function of time. The scale invariant solution to the mean-field problem is

$$\phi(\xi) = \alpha + \frac{\alpha\rho - 1}{\rho_o - \rho} - \frac{(\alpha\rho - 1)\rho_o}{\rho_o - \rho}\xi^{-1} \tag{16}$$

which represents the average diffusional interaction of a typical particle of size class ρ with all the other particles, as represented by the mean field, viz., $\phi = \alpha$ at $\xi = \rho_o$. The flux to or from the particle and the environment is

$$4\pi\xi^2\nabla\phi = 4\pi B(\rho) \tag{17}$$

and $B(\rho)$ is the stochastic counterpart to B_i as defined previously (see Equation 12) for an individual particle in the MDP formulation. If the gradient of ϕ is evaluated from Equation 16, then Equation 17 may be solved for $B(\rho)$ to yield

$$B(\rho) = \frac{(\alpha\rho - 1)\rho_o}{\rho_o - \rho} \tag{18}$$

$\alpha = 1$ and $\rho_o \to \infty$, so $B(\rho) = \rho - 1$ for the zero volume fraction.

Since $B = R^2\,\mathrm{d}R/\mathrm{d}t$, then the flux function for LSW becomes

$$\frac{\mathrm{d}R}{\mathrm{d}t} = \frac{1}{R}\left[\frac{R}{R_{\mathrm{AV}}} - 1\right] \tag{19}$$

Equation 19 shows that the average growth or shrinkage rate, $\mathrm{d}R/\mathrm{d}t$, of a typical particle depends on its size relative to the *average*, and that particles for which $R < R_{\mathrm{AV}}(\rho < 1)$ shrink, whereas particles for which $R > R_{\mathrm{AV}}(\rho > 1)$ grow. The general form of the flux function for non-zero volume fractions Q is

$$B(r) = \begin{cases} (\rho/\rho^* - 1)(1 - Q^{1/3})^{-1}, \rho > \rho^* \\ (\rho/\rho^* - 1)(1 - Q^{1/3}\rho/\rho^*)^{-1}, \rho < \rho^* \end{cases} \tag{20}$$

Solution of Equation 20 requires determination of ρ^* (or α) as a function of volume fraction Q. The distribution function $f(\rho, t)$ may be expressed in product

function form:

$$f(\rho, t) = g(\rho)h(t) \tag{21}$$

Values of α were found selfconsistently by iterating the solution for $g(\rho)$ subject to the requirement that the volume fraction [or equivalently the 3rd moment $g(\rho)$] is constant and that the 1st moment of the $g(\rho)$ distribution must be unity, or

$$\int_0^{\rho_{\max}} \rho g(\rho)\,\mathrm{d}\rho = 1 \tag{22}$$

Equation 22 arises from the fact that the variable ρ which occurs when $R = R_{\mathrm{AV}}$.

4. Classical theory of ripening (the LSW theory)

In order to understand the modern Ostwald ripening theories Voorhees [26] reviewed the classical LSW theory, which will be presented here. The LSW theory revealed both power-law growth and dynamic scaling, which are now considered universal characteristics of the kinetics of a first-order phase transition. This theory used the following assumptions:

(a) the coarsening second phase is spherical with redius R,
(b) the particles are fixed in space,
(c) the inter-particle distances between the particles are infinitely large compared with the particle radius, which means that there is no interaction among the particles, and the volume fraction Q of the dispersed phase is infinitesimally small (i.e. infinitely dilute system),
(d) both the particles and matrix are fluids, and
(e) the solute atoms diffuse to the spherical particles under steady-state condition.

The LSW theory has been widely adapted to determine the values of interfacial energy between the matrix and the dispersed phase since it provides a useful method to determine the values. Almost all the observed size distributions have been, however, broader than that predicted from the LSW theory.

The morphology of a dispersed spherical second phase will be characterized in terms of particle radius distribution $f(R, t)$, f is defined as the number of particles per unit volume at time t in a size class R to $R + \mathrm{d}R$. Representing a particle radius distribution in terms of continuous function $f(R, t)$ implies that there exists sufficient numbers of particles in the system for such continuum approach to be valid [26]. From the definition of f it is clear that $N(t) = f_{\mathrm{o}}$, where $N(t)$ is the number of particles per unit volume, and

$$f_n = \int_0^{\infty} R^n f(R, t)\,\mathrm{d}R \tag{23}$$

Thus, the flux of particles passing through a size class R to $R + \mathrm{d}R$ is $f \cdot \dot{R}$, where $\dot{R} = \mathrm{d}R/\mathrm{d}t$. Therefore, the time rate of change of f is given by a continuity equation of the form

$$\frac{\partial f}{\partial t} + \frac{\partial (f \cdot \dot{R})}{\partial R} = J \tag{24}$$

where J is a production term in particle size space. In the LSW theory, J is set to zero, which means that processes such as nucleation and particle coalescence, which introduce new particles of a given size class, are negligible. The flux of particle in size space is controlled by the function $\dot{R}(R)$. In the LSW theory, $\dot{R}(R)$ was determined by examining the growth or dissolution of an isolated spherical particle into a supersaturated medium.

The starting point of the LSW theory is the diffusion equation for the concentration C in the steady-state limit (or by employing quasistasionary approximation for the diffusion field in the matrix):

$$\nabla^2 \theta(R) = 0 \tag{25}$$

This determines the flow of material between particles, subject to the Gibbs-Thomson boundary condition at the surface of a particle of radius R.

Along the boundary conditions,

$$\theta(R) = \frac{1}{R} \tag{26}$$

$$\lim_{r \to \infty} \theta(r) = \theta_m \tag{27}$$

where θ_m is the supersaturation of the matrix during the Ostwald ripening [i.e., $\theta_m(t) \ll 1$]. Equation 26 is the dimensionless form of the linearized Gibbs-Thomson equation, assuming the ideal solution, for the solute concentration in the matrix at the surface of a spherical liquid particle. If the particle or matrix is solid, it is not posible to use Equation 26. By requiring flux conservation at the matrix-particle interface and that the particle is pure solute, Equation 25 with Equations 26 and 27 yields

$$\dot{R} = \frac{\theta_m - \dfrac{1}{R}}{R} \tag{28}$$

As a result of the quasistationary approximation is that this kinetic equation is valid for both growing and dissolving particles. Equation 28 shows that it is a mean field nature. This is a result of employing Equation 27 as a boundary condition, i.e. a particle grows or shrinks only in relation to a mean field concentration set at infinity.

The final element of the LSW theory is mass conservation. Mass or solute conservation must be explicitly added to the theory because Equation 28 is based on a solution to Laplace's equation, which does not conserve solute. Assuming that there are no sources of solute external to the system, solute conservation demands that the total solute content of the alloy be divided between the particle and matrix, viz.

$$\theta_o = \theta_m(t) + \lambda f_3(t) \tag{29}$$

where θ_o is the bulk alloy composition and $\lambda \equiv 4\pi/(3\Omega C_e)$. The parameter θ_m can be determined from Equation 29, and thus θ_m couples mass conservation into the kinetic equation. Instead of solving Equations 24, 28, and 29 for all times, the LSW theory found an asymptotic solution valid as $t \to \infty$.

The main problem is to reformulate the theory in terms of a double scaled variable $\rho \equiv R/\bar{R}$ where $\bar{R}$ is either the critical radius $R_C = 1/\theta_m$ (the particle with $\dot{R} = 0$) or the maximum particle size in the system [27]. Using the reformulated kinetic equation in conjunction with the solute conservation constraint, the LSW showed that as $t \to \infty$, the following should be true $K(t) = 3R_C^2 \dot{R}_C \to$ constant, $R_C \to \bar{R}$, and $f_3 \to \theta_o/\lambda$, where $\bar{R} = f_1 f_o$. Since the rate constant K is a constant at long times, a solution of the continuity equation of form $g(\rho)\, h(t)$ is possible for the particle size distribution function.

Using the asymptotic analysis the LSW treatment make the following predictions concerning the behavior of the two-phase mixtures undergoing Ostwald ripening in the long-time limit:

(a) The following temporal power laws are obeyed:

$$\bar{R}(t) = \left[\bar{R}^3(0) + \frac{4}{9}t\right]^{1/3} \tag{30a}$$

$$\theta_m(t) = \left[\bar{R}^3(0) + \frac{4}{9}t\right]^{-1/3} \tag{30b}$$

$$N(t) = \psi\left[\bar{R}^3(0) + \frac{4}{9}t\right]^{-1} \tag{30c}$$

$$\text{Where } \psi = \frac{\theta_o}{a\int_0^{3/2} \rho^3 g(\rho)\, \mathrm{d}\rho} \tag{30d}$$

and t is defined as the beginning of coarsening in the long-time regime.

The prefactor 4/9 is the dimensionless coarsening rate, and the overbar denotes an average. The exponents are independent of the material and the history of the sample, and the amplitudes depend on a few material constants but are also independent of initial conditions.

(b) The asymptotic state of the system is independent of the initial conditions. Furthermore, the particle radius distribution is self-similar under the scaling of the average particle size. In addition to this prediction, an analytic form for the particle distribution function was obtained:

$$f(R,t) \propto \frac{g\left(\dfrac{R}{\bar{R}}\right)}{\bar{R}^4} \tag{31}$$

for late times. This time-independent distribution function $g(\rho)$ is calculable and is shown in Fig. 1.

The LSW predicts that after long times the distribution of particle sizes, probably scaled, should reach a universal form that is independent of all materials parameters. Qualitative features of this theory have been confirmed [36], but as shown in Fig. 1 measured particle size distributions are more broad and squat [28–31, 37–40] than the LSW theory.

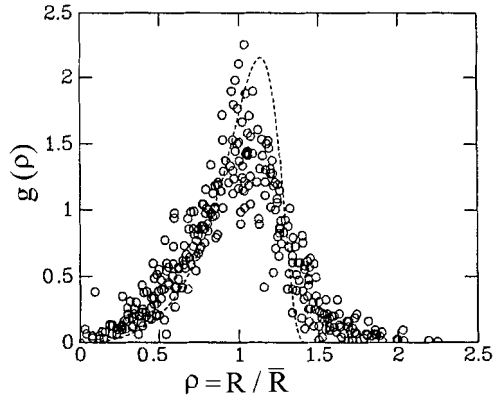

Figure 1 Indicates that particle size distributions [16] from different alloys [28–35] are broader than predicted by the mean-field theory of the LSW model.

5. Progress in Ostwald ripening theories: modern Ostwald ripening theories

Soon after the publication of the LSW papers, many experimentalists rushed to test the veracity of the theory. The experimental results have confirmed the prediction of self-similar coarsening behavior at long-times; however, virtually none of the reported distributions are of the form predicted by the LSW theory (see Fig. 1). The reported distributions are generally broader and more symmetric than the LSW predictions (Fig. 1; also see [41, 42]).

It was realized early that a major problem with the LSW approach was the mean field nature of the kinetic equation. Such a mean field approximation assumes that a particle's coarsening rate is independent of its surroundings, i.e., a particle with nearest neighbors which are larger than itself will coarsen at exactly the same rate as if it were surrounded by particles that were of a smaller radius. The LSW assumed that their deterministic rate equation would be valid at an unspecified low volume fraction of ripening phase. This flaw (i.e. the diffusional interactions between particles) in the LSW approach was recognized, and advanced as the cause for the apparent disagreement between the theoretically predicted and experimentally measured particle size distributions [14]. The strength of the diffusional interactions between particles stems from the long range Coulombic nature of the diffusion field surrounding a particle. As a result, particle interactions occur at distances of many particle diameters and restrict the validity of LSW theory to the unrealistic limit of zero volume fraction of coarsening phase. The LSW theory was difficult to be test rigorously by experiment or numerical simulation. Experiments typically study volume fractions appreciably larger than zero.

Efforts to modify works on extending the theory of LSW to nonzero Q has been attemted by many groups [8–18, 43–46], using both analytic and numerical methods. In order to remove the zero volume fraction assumption of the LSW theory, one needs to determine

the statistically averaged diffusional interaction of a particle of a given size class with its surroundings. Many of the attempts to determine the statistically averaged growth rate of a particle either do not account for the long-range nature of the diffusion field surrounding the particle [3, 8, 10], and/or employed *ad hoc* assumptions in an attempt to account for the diffusional interactions between particles [4, 15]. Brailsford and Wynblatt (The BW theory) [9], Voorhees and Glickman (The VG theory) [13, 14], Marqusee and Rose (The MR theory) [12], and Tokuyama and Kawasaki (the TK theory)) [18], have proposed more realistic models of the Ostwald ripening process at finite-volume fractions of coarsening phase.

For the most part, analytic extensions have been based either on *ad hoc* assumptions (the Ardell theory or the MLSW theory [8, 46] and Tsumuraya and Miyata (the TM theory) [11]), or on perturbative expansions in Q, typically taken to order $\sqrt{Q}$ (the work of Marqusee and Rose (the MR theory) [12] and Enomoto, Tokuyama and Kawasaki (the ETK theory) [17]). In addition, a theory was developed by Marder [16] in which two-particle correlations were included for three-dimensional Ostwald ripening. All these approaches lead to the following growth law:

$$\bar{R}(t) = [\bar{R}^3(0) + K(Q)t]^{1/3} \tag{32}$$

where $\bar{R}(0)$ is the average radius at the onset of coarsening, and the coarsening rate $K(Q)$ is a monotonically increasing function of Q. The particle-size distribution function satisfies

$$f(R, t) \propto g(\rho, Q)/\bar{R}^{(d+1)} \tag{33}$$

where $\rho \equiv R/\bar{R}$, d is the dimensional number. The theories predict a broadening of $g(\rho, Q)$ as the volume fraction is increased. Unfortunately, the perturbative theories can neither go beyond $\vartheta(Q)$ nor be applied to two-dimensional systems, and the *ad hoc* approaches contain uncontrolled approximations.

According to the author's knowledge, two numerical studies have been conducted in three dimensions. Voorhees and Glickman (The VG theory) [13, 14, 26] carried out a numerical simulation, by a novel approach based on Ewald-sum techniques, reviewed in Section 5.7. In the following sections the some of the important modern Ostwald ripening theories will be reviewed in detail: in the cronological order, (a) The Ardell theory (the MLSW theory) [8]; (b) the Brailsford-Wynblatt (BW) theory [9]; (c) Davies-Nash-Stevens (LSEM) theory [10]; (d) the Tsumaraya-Miyata (TM) theory [11]; (e) the Marqusee-Ross (MR) theory [12]; (f) the Tokuyama-Kawasaki (TK) theory [18]; (g) the Voorhees-Glicksman (VG) theory [13, 14]; (h) the Enomoto-Tokuyama-Kawasaki (ETK) theory [17]; (i) the Yao-Elder-Guo-Grant (YEGG) theory [15].

5.1. The Ardell (MLSW) theory (1972)

Ardell [14] established first that the LSW theory correspond to the limit $Q \to 0$ and proposed a modified LSW particle growth rate equation for $Q \neq 0$. Therefore, the MLSW theory has been developed to include the effect of Q on diffusion-controlled coarsening kinetics. In Ardell's modified LSW theory he changed the diffusion geometry and hence modified the kinetic equation. The Gibbs-Thomson value for the solute concentration at the particle surface is used, as in the LSW theory, but the average solute concentration of the matrix is not set at infinity but on the surface of a sphere centred on the particle and having a radius essentially equal to half the mean particle spacing. This radius decreases with increasing volume fraction giving rise to the volume fraction effect.

The result showed that coarsening rate increased with volume fraction and the theoretical size distribution broadened rapidly with increasing volume faction. The rate of change of the average sized particles was still proportional to $t^{1/3}$ (see Equation 33). This modified LSW theory (MLSW theory) included the LSW theory in the limit of zero volume fraction.

This so-called modified LSW (MLSW) theory predicts that the average particle radius, $\bar{R}$, should increase with time, t, according to the equation

$$\bar{R}^3(t) - \bar{R}^3(0) = K(Q)t \tag{32}$$

where $K(Q)$ is a volume-fraction dependent rate constant given by

$$K = \frac{6\gamma D C_e \Omega^2 \rho_m^3}{\upsilon R_B T} \tag{34}$$

where

$$\upsilon = \frac{3\rho_m^2}{1 + 2\beta\rho_m - \beta} \tag{35}$$

$$\beta = \frac{6Q^{1/3}}{\mathrm{e}^{3Q}\Gamma(Q)} \tag{36}$$

and

$$\rho_m = \frac{(\beta^2 + \beta + 1)^{1/2} - (1 - \beta)}{\beta} \tag{37}$$

where ρ_m is the theoretical relative maximum particle size of the polydisperse assembly, and

$$\Gamma(Q) = \int_{8Q}^{\infty} x^{-2/3}\,\mathrm{e}^{-x}\,\mathrm{d}x \tag{38}$$

The parameters ρ, ρ_m and υ all depend upon the volume fraction (Q) of the precipitate particle through the parameter β defined in Equation 36, which accounts for the implicit dependence of K upon Q in Equation 34. To facilitate the comparison between the MLSW theory and experimental data and the effect of Q on the coarsening rate, it is convenient to plot the ratio $K(Q)/K(0)$, where

$$K(0) = \frac{8\gamma C_e D \Omega^2}{9 R_B T} \tag{39}$$

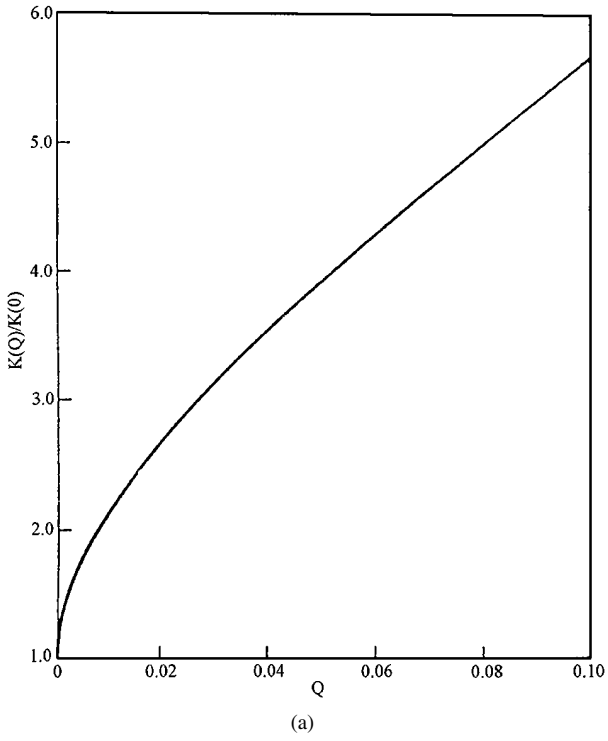

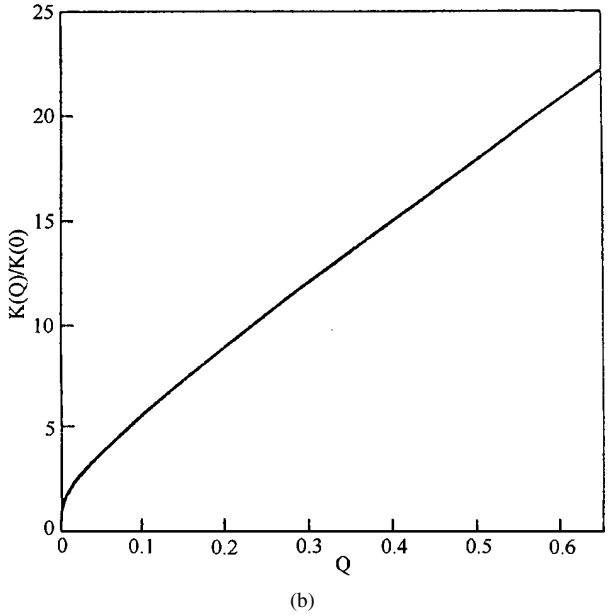

Figure 2 Illustrating how the rate constant, $K(Q)$, in the MLSW theory, for diffusion-controlled coarsening [8] varies with the volume fraction Q of the second phase; (a) at small volume fractions, (b) at volume fractions up to $Q = 0.65$.

as a function of Q. The ratio

$$\frac{K(Q)}{K(0)} = \frac{27}{4}\frac{\bar{\rho}^3(Q)}{\upsilon(Q)} \tag{40}$$

is shown in Fig. 2a for small volume fractions, and in Fig. 2b for volume fractions up to 0.65. It is seen in Fig. 2a that even at small values of Q, the effect of Q is appreciable.

The coarsening rate is twice that of the LSW theory when Q is only about 0.08, a factor of three times as great when Q is only about 0.027, which are unreasonable when compared with the experimental data.

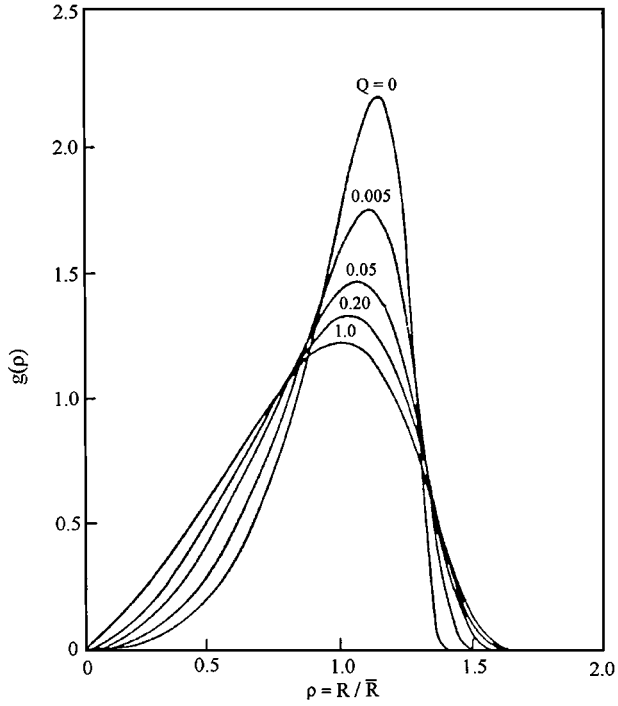

Figure 3 Illustrating the dependence of the theoretical distribution of particle sizes on the volume fraction (according to the MLSW) [8].

The MLSW theory predicts that the distribution of particle sizes obeys the following equation

$$g(\rho) = \frac{-3\rho^2}{\theta(\rho)} \exp\left[\int_0^{\rho_m} \frac{3x^2\,\mathrm{d}x}{\theta(x)}\right]; \quad \rho \leq \rho_m$$
$$= 0; \quad \rho > \rho_m \tag{41}$$

where $$\theta(\rho) = (\rho - 1)(1 - \beta\rho)\upsilon - \rho^3 \tag{42}$$

The function $g(\rho)$ is independent of time and depends implicitly upon Q through the Q-dependent parameters β and υ in Equation 42.

Fig. 3 shows the predicted size distribution $[g(\rho)]$ as a function of Q. The greatest change in $g(\rho)$ occurs for small values of Q, as illustrated by the curves for $Q = 0.005$ and 0.05. When Q is greater than 0.2, the shape of the distribution curve becomes relatively insensitive to Q.

Chelman and Ardell [32] have attempted to explain the broadness of the histograms in Ni-Cr-Al and Ni-Al alloy systems by use of the MLSW theory. They [32] find however the absence of the volume fraction effect on the broadness in these alloys even if the volume fraction was between 0.09 and 0.60. They concluded that coarsening in these cases was not controlled by the MLSW theory but instead by the original LSW theory.

5.2. The BW theory (1979)

Brailsford and Wynbladt [9] have developed a theory of particle coarsening, assuming that the growth rate of the particle of one size class is a function of the entire particle size distribution and the prevailing concentration gradient around the particle. The growth rate so

developed was less sensitive to volume fraction than the MLSW theory but more sensitive than the LSEM theory (See Section 5.3).

Because of the discrepancy between the MLSW theory and experiments Brailsford and Wynblatt [9] have re-investigated the volume fraction-sensitive particle coarsening. In this investigation the problem was divided into two parts: (a) the determination of the radial growth rate of a particle embedded in a configurationally random array of particles of like nature but different sizes, and (b) the solution of continuity equations for the particle size distribution, neglecting the possibility of coalescence of large particles as the coarsening proceeds.

In the BW theory the growth rate is determined by a continuous medium having a homogeneous loss rate and homogeneous production rate of solute atoms. The kinetic equation is given in the form of LSW theory:

$$\bar{R}^3(t) - \bar{R}^3(0) = K(Q)t \tag{32}$$

where

$$K = \frac{6\gamma\Omega D C_e}{R_B T \alpha}\left(\frac{\bar{R}}{R^*}\right)^3 \tag{43}$$

where α and R^* are given in Equations 31 and 49 in [9] and R^* is the critical radius at the onset of coarsening.

The results of BW theory are more acceptable than those of the MLSW theory, the rate constant being increased by a factor of about 3.5 relative to the LSW approximation for a volume fraction of 0.5. The particle size distribution function is broadened but the theory does not give as broad a range of sizes as the LSEW theory.

Results obtained by this procedure for the asymptotic particle size distribution, the ratio of $\bar{R}/R^*$ and for the rate constant K as function of Q are given in Figs 4 and 5, respectively. For the sake of comparison, the results of prior inestigations of the volume fraction dependence of the rate constant are also incorporated in Fig. 5.

Ardell and co-workers [30, 32] studied coarsening behavior in several Ni-base superalloys in which the ripening rate constants were determined at different volume fractions. In the earlier work by Ardell and

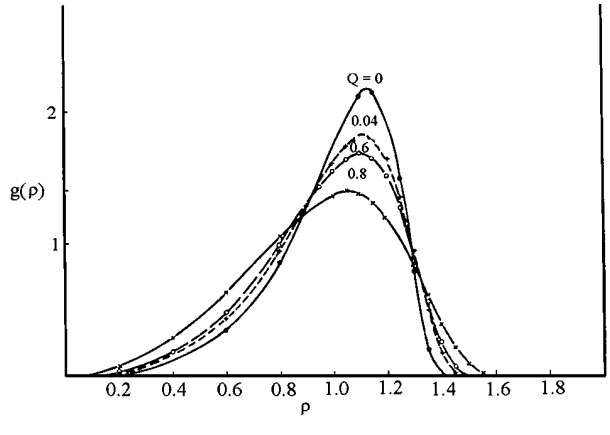

Figure 4 BW distribution function $g(\rho)$ for the MLSW model as a function of ρ for different volume fractions, Q, where $\rho = R/R^*$ [9].

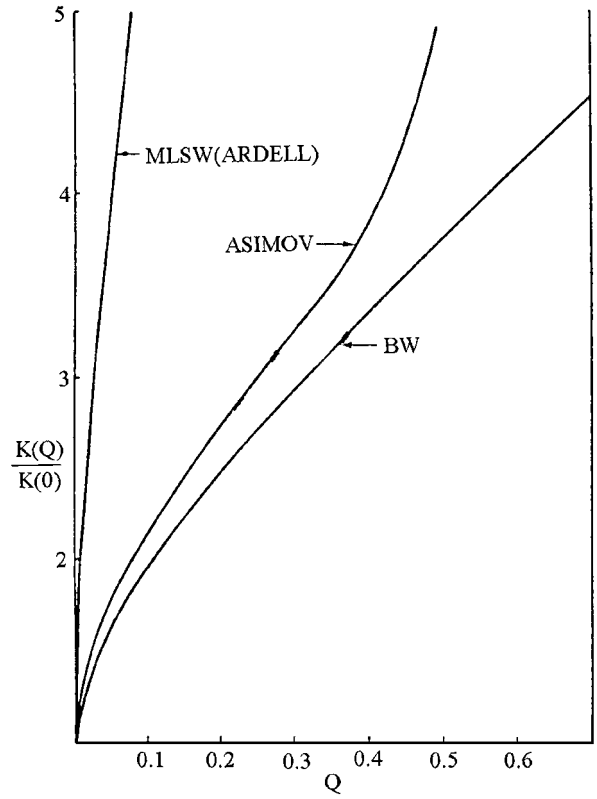

Figure 5 The variation of the rate constant $K(Q)/K(0)$ with volume fraction Q in the BW Theory [9]. The curves from MLSW and Asimov [4] models were also included for comparison.

Nicholson [30] the growth kinetics of $Ni_3Al(\gamma')$ precipitates in Ni-Al alloys were measured for volume fractions ranging from ≈0.09 to ≈0.20. The BW model predicts an increase in rate constant of ≈31% over this range of volume fraction while the data fall within the scatter band which represents about a factor of 2 in K [30].

5.3. The LSEM theory (1980)

The central idea in the LSEM theory [10] is that of "*encounters*" between growing particles. According to the LSEM theory, if, during the coarsening process, a significant amount of second-phase particles is present, the interaction between the diffusion field around two growing particles may bring their surfaces together causing them to coalesce. When a large particle approaches, the diffusion field of the larger particle dominates over that of the smaller particle, resulting in a rapid dissolution and coalescence. Such a coalescence of particles increases the growth rate to a small extent and broadens the particle-size distribution, although the rate of change of the mean particle size remains proportional to the cube root of the aging time. The LSEM theory also predicts the particle-size distribution to be more symmetrical and broader compared with that predicted by the LSW theory. The coalescence of Ni_3Al particles in an Ni-Co-Al system, in the form of "necks" and L-shaped particles, has been reported by Davies *et al.* [10], suggesting the occurrence of the "encounter" process.

The LSEM showed that the effect of encounters increases the growth rate by a factor of approximately

three and altered the shape of particle size distribution making it symmetrical over the whole volume fraction range, although the rate law is unaffected by the encountering effect. The predicted particle size distribution of the encountering theory was compared with an experimental histogram of encountered Ni_3Al type precipitates in a Ni-Al-Co alloy [10]. In that particular example it was shown that peak height, broadness, and general shape of the size distribution were reproduced by the theory.

In the LSEM theory the kinetic equation is as follows:

$$\bar{R}^3(t) = \bar{R}^3(0) + \frac{6\gamma\Omega C_e D\bar{r}'^3}{R_B T Y} t \qquad (44)$$

where C_e is the average mole fraction of solute in the matrix, and $\bar{r}'^3$ and Y are the parameters obtained from the LSEM analysis and depend on volume fraction of precipitate.

Lifshitz and Slyozov show that Y must be constant and this is also true in the LSEM theory. In the zero volume fraction approximation Y is shown to be equal to 27/4 and the mean particle radius is equal to the critical radius. The value of Y is changed in the LSEM theory and in principle it can not be assumed that the average particle radius and the critical radius are the same as in the unmodified theory. With $\bar{r}'^3 = 1$ and $Y = 27/4$ Equation 44 reduces to the familiar equation of the LSW theory but in the LSEM theory the $\bar{r}'^3$ and Y values have to be determined.

In Fig. 6 Y is plotted as a function of Q. It can be seen that Q diminishes rapidly from its value of $27/4 = 6.75$ at $Q = 0$ initially and then decreases more slowly. Fig. 6 also shows the ratio of the rate constant K for a volume fraction Q [$K(Q)$] to that for $Q = 0$ [i.e. $K(0)$]; $K(Q)/K(0)$. This ratio is a direct measure of the degree to which encounters increase the rate of coarsening. Inspection of Equation 44 shows that this ratio is given by $6.75\,\bar{r}'^3/Y$, 6.75 being Y for $Q = 0$, for which value $\bar{r}' = 1$. It can be seen that the coarsening rate varies by a factor of a little less than three over the whole volume fraction range.

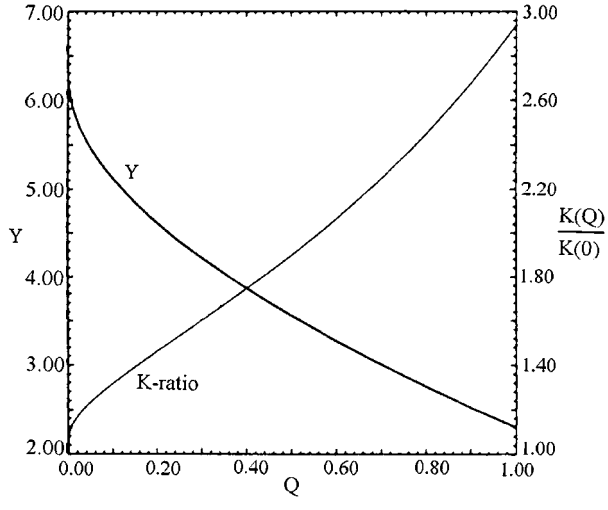

Figure 6 The effect of volume fraction Q on the parameter Y and the ratio of the rate constant $K(Q)/K(0)$ for the LSEM model [10].

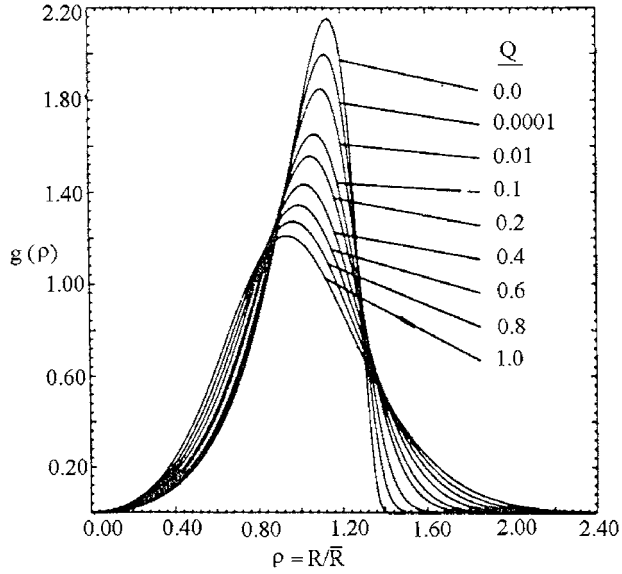

Figure 7 LSEM particle size distribution as a function of precipitate volume fraction Q [10].

Assuming the effective diffusion coefficient D in the growth-rate equation (Equation 44) may be given by an Arrhenius type equation using the LSEM analysis

$$\mathrm{Log}\left[\frac{KT}{C_e}\right] = \mathrm{Log}\left[\frac{6\gamma\Omega^2\bar{r}^2 D_o}{R_B Y}\right] - \frac{A}{2.3R_B T} \qquad (45)$$

Thus plots of $\mathrm{Log}(KT/C_e)$ versus $1/T$ yield the activation energy A for coarsening from the slope and D_o from the intercept.

Fig. 7 shows the particle size distribution function for various values of Q predicted by the LSEM theory. The effect of increasing volume fraction is to progressively flatten and broaden the distribution and skew it in the opposite sense to the unmodified distribution.

The advantage of the LSEM theory over the MLSW theory is that its modification of the LSW theory is properly incorporated into the statistical framework of the theory with no implicit statistical assumption that can not be given some justification. We also note that the LSEM theory gives considerably broader relative size distributions than the MLSW theory and this also accords better with experiment.

5.4. The TM theory (1983)

Tsumuraya and Miyata [11] developed six models for steady-state particle coarsening in order to explain the shapes of experimentally obtained particle size distribution histograms. The models are developed for coarsening process controlled by volume diffusion compelled by reduction of interfacial area between particles and matrix. The particle size distributions and coarsening rates are presented for each model. The basic $t^{1/3}$ rate law is maintained in all models.

In the TM treatment it is dealt with the concentration gradients around the individual particle depending on the types of spatial distribution of particles in solids. The particle size distributions and growth rates of average particle size are also derived. The growth rate of

average particles can be given by

$$\frac{d\rho}{d\tau'} = -p = \frac{1}{3}\left[\frac{\rho - 1}{\rho^3} f'\upsilon - \rho\right] \tag{46}$$

where $\rho = R/R^*$, R^* is the critical radius for ripening, f' is a function in the concentration gradient in the present model. Ardell [8] also used the critical radius instead of the average radius $\bar{R}$, which is the one which is neither dissolving nor growing during coarsening and increases with time.

$$\tau' = \ln\left(R^{*3}\right) \tag{47}$$

$$\upsilon = \frac{3\vartheta D\Omega}{C_B}\frac{dt}{dR^{*3}} \tag{48}$$

The expression for υ contains a parameter ϑ which is given by

$$\vartheta = \frac{2\gamma\Omega C_e}{R_B T} \tag{49}$$

where C_B is the atomic fraction of the solute atoms dissolved in the precipitates.

The normalized equation to represent the particle size distribution $h(\rho)$ is given by

$$h(\rho) = \frac{e^{-\Phi}}{p} \tag{50}$$

where

$$\Phi = \int_0^p \frac{1}{p}\, d\rho \tag{51}$$

and the equation for p has been given in Equation 46.

The rate law of the average particle size can be expressed by

$$\bar{R}^3(t) - \bar{R}^3(0) = K(Q)t \tag{32}$$

where $K(Q)$ is the rate constant given by

$$K(Q) = \frac{3\vartheta D\Omega\bar{\rho}^3}{\upsilon} \tag{52}$$

The rate of the average particle size is proportional to the cube root of time (i.e. $t^{1/3}$) in all the present models. This is caused by employement of the linearized Gibbs-Thomson equation and the volume diffusivity at steady-state condition. The ratio of $K(Q)$ to $K(0)$ becomes

$$\frac{K(Q)}{K(0)} = \frac{27}{4}\frac{\bar{\rho}^3}{\upsilon C_B} \tag{53}$$

since

$$K(0) = \frac{4\vartheta D\Omega C_B}{9} \tag{54}$$

The volume fraction effect is physically due to the interaction between the particles through the distance between the particles, i.e. statistical nearest neighbor effect. The thickness of the matrix influences the interaction between the particles. The interaction leads to an increase of the coarsening parameter $K(Q)/K(0)$ which is shown in Fig. 8.

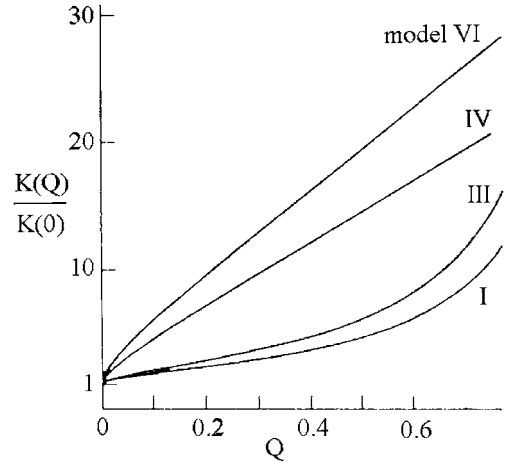

Figure 8 The changes of the ratios $K(Q)/K(0)$ in each TM model [11] for different volume fraction ranges, Q.

In conclusion, in the TM theory six models have been developed, which incorporate both the diffusion geometry and the volume fraction of the particles to explain the broadness of the experimental size distribution histograms. The models are produced so as to reflect the real spatial particle dispersion. One of the six models is a modified version of Ardell's model [8].

Tsumuraya and Miyata [11] compared the available experimental distribution histograms at steady-state condition controlled by volume diffusion and have classified them into two of the proposed models. Model III has explained the broadness of the published histograms in the Ni-Al : $Q > 0.1$ and Ni-Cr-Al : $Q > 0.2$ alloys. The spatial distribution of precipitates in these alloys has shown a periodic array of precipitates in cube directions. Model VI, where each particle with various sizes distributes randomly so particle interpenetration is excluded, has also explained the broadness of size distribution histograms in Ni-Al : $Q < 0.1$, Ni-Cr-Al : $Q < 0.2$, Fe-Ti-Si : $Q = 0.045$–0.06, Co-Ni-Cr-Ti : $Q = 0.10$–0.17 and Ni-Si : $Q = 0.045$ alloys. These are alloys with smaller volume fractions of precipitates.

5.5. The MR theory (1984)

The purpose of this work [12] is to extend the theory of Ostwald ripening to nonzero volume fractions as other modern theories. Using studies in the theory of diffusion controlled reactions [47–51] Marqusee and Rose [12] derived a growth law for a particle in the presence of other particles and solve for the asymptotic distribution function by the techniques developed elsewhere [52]. It was found that the distribution function assumes a unique asymptotic form independent of initial conditions but dependent on the final equilibrium volume fraction. The exponents in the temporal power laws are unchanged by the competitive effects but the amplitudes have significant volume fraction dependence, at volume fractions as small as 1%. The growth law and the amplitudes for the temporal power laws deviate from their values in the limit of zero volume fraction. Overall, the distribution function is broadened by

the competition, which leads to more rapid coarsening rates.

To develop a growh law for this work let us consider the particles of the minority phase as spherical particles of radius R surrounded by the majority phase which is characterized by the concentration field $C(r, t)$. The radius of a given particle increases by the incorporation of mass into it and, by mass balance, there is an associated decrease in the concentration field. The growth rate of a particle is calculated under the assumption that it is diffusion limited and stationary. In the limit of zero volume fraction of particles, the dilute limit, competition between particles can be neglected and we need to consider only one particle. The growth rate is obtained by solving for the steady state flux into (or out of) a particle, subject to the constraint that the interface is at local equilibrium. Thus the concentration field satisfies the following equation

$$D_o \nabla^2 C(r, t) = 0 \tag{55}$$

and the boundary condition

$$C(r, t)|_R = C_{eq}(R) \tag{56}$$

Where R is the radius of the particle with center at the origin, D_o is the diffusion coefficient for the concentration, and $C_{eq}(R)$ is the equilibrium concentration associated with a particle of radius R. For a concentration of C_e at infinity, the solution to Equation 55 is

$$C(r, t) = C_e\left[1 - \frac{R}{r}\right] + C_{eq}(R)\frac{R}{r} \tag{57}$$

For a spherical particle and ideal solution, the R dependence of $C_{eq}(R)$ (i.e. the Gibbs-Thomson equation) is

$$C_{eq}(R) \cong C_{eq}(\infty)\left[1 + \frac{l_C}{R}\right] \tag{58}$$

with $l_C = 2\gamma\Omega/R_B T$ (see Equation 2)

where $C_{eq}(\infty)$ is the concentration in equilibrium with a macroscopic particle.

The presence of a particle at the origin creates a long range perturbation in the concentration field, which decays as $1/R$, and which produces a nonanalytic density dependence in the growth law for the case where competition among particles are considered.

The total flux mass into a single isolated particle is

$$J_T = 4\pi D_o[C_o - C_{eq}(R)] \tag{59}$$

A variety of techniques have been used in the theory of diffusion controlled reactions to treat this case of competition among particles. Here a multiparticle scattering (MPS) approach, which have been applied by a number of authors [48–51], is used in this work. These results are generalized to the case of a distribution of particle sizes and the boundary condition given in Equation 56. In this approach, an equation is written for the microscopic concentration field for an ensemble of particles located at positions $\{r_i\}$. This equation is then averaged with respect to the position of the particles and compared to the macroscopic equation in the form of a multiple scattering series, from which the growth law is obtained.

Rather than solve the steady state diffusion Equation 55, subject to the boundary condition Equation 56, a set of sink terms is introduceed, one at each position of the particles. The microscopic concentration field [12] obeys the equation

$$D_o \nabla^2 C(r, t) = \phi(r) + \sum_{i=1}^{N} B_i \delta(r - r_i) \tag{60}$$

where the set $\{B_i\}$ denotes the strength of the sinks located at positions $\{r_i\}$ and are functions of the particle positions and their radii, $\phi(r)$ is an auxiliary field function introduced to account for external boundary conditions.

The growth rate $V(R_1, \bar{C})$ for a particle of radius R in the present treatment is

$$V(R_1, \bar{C}) = \dot{R} = \frac{D_o\Omega}{R}\left[\bar{C} - C_{eq}(R)\right]\left[1 + R\sqrt{4\pi\rho\langle R\rangle}\right] \tag{61}$$

where $\rho\langle R\rangle$ is the average number density with respect to the particle size distribution.

The competition increases the diffusion controlled reaction rate and the deviation from the dilute limit goes as the square root of the density.

From the growth law (see Equation 61), it is possible to derive the asymptotic distribution function for particle sizes. Here a time scaling technique is used, which allows the extraction of the temporal power laws; the reduction of the problem to the solution of a simple first order differential equation; and imposition of self-consistent constraints on the zeroth and first moments of the distribution function. It is here assumed that the distribution function $n(R, t)$ for the number of particles with radius R per unit volume can only be changed by growth or dissolution of particles. In this case, it must obey a continuity equation in R space,

$$\frac{\partial n}{\partial t}(R, t) + \frac{\partial}{\partial R}V[R, \bar{C}(t)]n(R, t) = 0 \tag{62}$$

where $V[R, \bar{C}(t)]$ is given by Equation 61. It is also assumed that the particles are stationary. Note that $n(R, t)$ is normalized to the density of particles and not to one. Thus the density is

$$\rho(t) = \int_0^\infty n(R, t)\,\mathrm{d}R \tag{63}$$

and it changes with time. Nucleation is neglected in Equation 62, since it is concerned with the late stages of phase seperation.

Before introducing the time scaling, we transform to the reduced variables

$$a = R/l_C; \quad \tau = t D_o \Omega C_{eq}(\infty)/l_C^2$$
$$\sigma(\tau) = \frac{\bar{C}(t) - \bar{C}_{eq}(\infty)}{\bar{C}_{eq}(\infty)} \tag{64}$$

The distribution function $F(a, \tau)$ in the long time limit in the scaled form is

$$F(a, \tau) = \tau^{-y} F_o(z) \tag{65}$$

where

$$z = a\tau^{-x} \tag{66}$$

where the exponents x and y are variables and are determined elsewhere [12]. In the long time limit, complete phase separation must be reached. This implies that $\sigma(\tau)$ must vanish in this limit. To satisfy this condition for the approach to equilibrium, we should have

$$\int_0^\infty z^3 F_o(z)\, dz = 1 \tag{67}$$

which serves as a normalization condition. It can be determined that the supersaturation $\sigma(\tau)$ decay to zero as τ^{-x}. Thus in the late stages of phase separation

$$\sigma(\tau) = \sigma_1 \tau^{-x}; \quad \langle a \rangle = a_o \tau^x; \quad \bar{\rho}(\tau) = \rho_o \tau^{-3x} \tag{68}$$

So σ_1, a_o and ρ_o are defined in Equation 68. To obtain the distribution function, the amplitude for the decay of supersaturation σ_1 should be determined. Also the amplitudes for the average radius $\langle a \rangle$ and density of particles $\bar{\rho}(\tau)$, a_o and ρ_o, should be calculated self-consistently. The constraints on σ_1 yield its value as well as the cutoff z_o where the particle distribution vanishes.

Therefore, the distribution function can be written as

$$F_o(z) = \frac{C_o}{(z_o - z)^{\alpha'}} \frac{1}{\left(z + 3/z_o^2\right)^{\beta'}} \exp\left[-\frac{\delta'}{z_o - z}\right] \qquad z \le z_o$$
$$= 0 \qquad z > z_o \tag{69}$$

where z_o is the cutoff value where the particle size distribution vanishes. α', β' and δ' are function of z_o,

$$\alpha' = 2 + \frac{3z_o\left(6 + z_o^3\right)}{\left(z_o^3 + 3\right)^2}; \quad \beta' = 1 + \frac{27}{\left(3 + z_o^3\right)^2};$$
$$\delta' = \frac{3z_o^4}{\left(3 + z_o^3\right)} \tag{70}$$

and C_o is the normalization constant determined by Equation 3.17 in [12].

The results [12] for zero volume fraction and the lowest order correction which may be obtained analyically (in the dilute limit) are:

$$z_o = \left(\frac{3}{2}\right)^{1/3}; \quad \alpha' = \frac{11}{3}; \quad \beta' = \frac{7}{3}; \quad \delta' = \left(\frac{3}{2}\right)^{1/3} \tag{71}$$

which are agreement with previous results [13, 14, 52]. This yields in the dilute limit the power law

$$\langle a \rangle = \left(\frac{4}{9}\right)^{1/3} \tau^{1/3}; \quad \sigma(\tau) = \left(\frac{9}{4}\right)^{1/3} \tau^{-1/3};$$
$$\bar{\rho}(\tau) = 1.99\tau^{-1} \tag{72}$$

Note that the supersaturation $\sigma(\tau)$ and the average radius $\langle a \rangle$ are the inverse of each other. The inverse of the supersaturation is by definition the critical radius, above which particles grow and below which particles dissolve. Thus we obtain the well-known result that the average radius is equal to to critical radius. This will not be true at finite volume fractions. From the calculations [12] the following parameters can be obtained

$$\sigma_1 = \left(\frac{9}{4}\right)^{1/3} \left[1 - 0.815\sqrt{Q_\infty} \ldots .\right]$$
$$z_o = \left(\frac{3}{2}\right)^{1/3} \left[1 + 1.222\sqrt{Q_\infty} \ldots .\right] \tag{73}$$
$$a_o = \left(\frac{4}{9}\right)^{1/3} \left[1 + 0.740\sqrt{Q_\infty} \ldots\right]$$

where Q_∞ is the equilibrium volume fraction of the second phase particles. It can be seen in Equation 73 that the leading order corrections are all of the order of the square root of the volume fraction. They predict that the average radius grows more rapidly, that the distribution function broadens, and that the decay rate of the concentration decreases. Also, the average radius and the critical radius are no longer equal.

The analytic form of the distribution function (Equation 69) was calculated for volume fractions up to $Q_\infty = 0.15$ by the iterative approach. The resulting distribution function is plotted for a series of volume fractions in Fig. 9. Note that since the distribution function is normalized according to Equation 3.17 in [12], the curves have very different heights. The effect of competition shifts the maximum of the distribution function to higher values of z and broadens it. We see that there are significant changes in the scaled distribution function at very low volume fractions. Tradationally, the distribution function when determined experimentally [23] is reported in the units of the average radius and

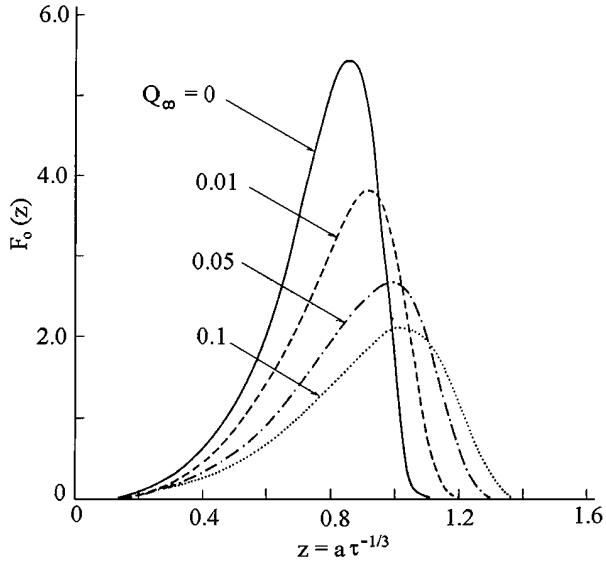

Figure 9 Plots of the scaled particle size distribution function $F_o(z)$ versus the scaled radius $z = a\tau^{-1/3}$ in the MR model (Plots are given for equilibrium volume fractions $Q_\infty = 0$ [12], $Q_\infty = 0.01$ (- -), $Q_\infty = 0.05$ (----), and $Q_\infty = 0.1$ (. . .) [12].

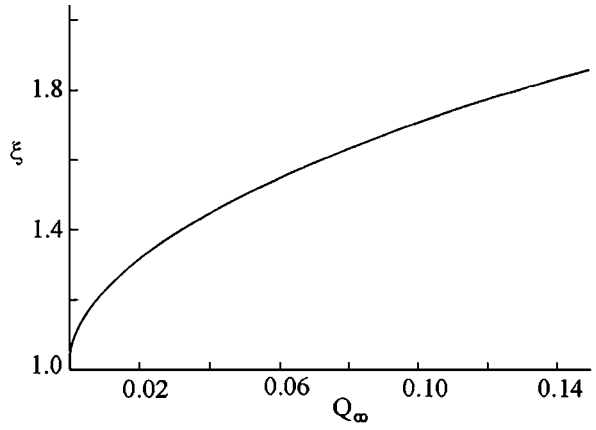

Figure 10 Plots of the reduced coarsening rate $\xi[=\langle a(Q_\infty)\rangle^3/\langle a(0)\rangle^3]$ versus the volume fraction Q_∞ (12).

normalized by the density of particles. The differences in the distribution function at various volume fractions will appear smaller when presented this way than in Fig. 9.

To see clearly the increase in the coarsening rate, Fig. 10 is plotted in which the cube of the average radius divided by its dilute limit $\xi(Q_\infty)$:

$$\xi(Q_\infty) = \frac{\langle a(Q_\infty)\rangle^3}{\langle a(0)\rangle^3} \tag{74}$$

The cube of the average radius is linear in time and is a frequently measured characteristic of the distribution. The greatest increase occurs in the first few volume percent, followed by a slower increase.

5.5.1. Comparison of the MR theory with the other theories

In the MR theory the effect of competition among particles causes a significant increase in the coarsening rate. In this model, as in the dilute case, the average radius grows as $t^{1/3}$ and the density of particles of the minority phase decreases as t^{-1}. The changes due to competition appear in the amplitudes for the temporal power laws and the first order deviations from their dilute values go as the square root of the volume fraction $\sqrt{Q_\infty}$. Other theoretical works such as TM, MLSW, BW theories on the coarsening at finite volume fractions has approached the problem of competitive effects in a variety of ways. Contrary to the MR theory, they found that the coarsening rate could either increase or decrease as volume fraction increased depending on the configuration of particles being considered. These results are due to the particular configurations they considered.

The TM and MLSW theories have proposed *ad hoc* corrections to the growth law that permit solutions for the asymptotic distribution by the method of LSW theory. These approaches assume the flux into or out of a particle is increased at finite volume fractions and consequently find an increase in the coarsening rate. These theories predict increases that are much larger than the MR theory. The results for the BW theory are qualitatively similar to the MR theory but differe quantitatively. The BW model derives a density dependent growth rate by an "effective medium" argument and solve for the asymptotic distribution function by the technique of LSW. No analytic first order corrections to the time dependence of either the density or average radius is given. The approximations involved in the derivation of the growth law in the BW work are uncontrolled and for mathematical simplicity, and *ad hoc* interpolation formula is used. None of the previous theoretical work has approached the problem for a systematic statistical mechanic point of view as attemted in the MR work.

5.6. The TK theory (1984)

Tokuyama and Kawasaki [18] have developed a new statistical-mechanical theory of diffusion-controlled particle ripening for finding the system of kinetic equations at the non-zero volume fractions of second phase particles, to order $\sqrt{Q}$. They pointed out that the *collisionless drift process* and *soft-collision process* play important roles for competitive growth in coarsening. The soft-collision process has been studied by the none of the previous authors except the MR and TK theories. The soft-collision process originates from the interactions between particles which are immobile but are correlated. Such correlations are generated by long time cumulative effects of particle interactions through the diffusion field. This is analogous to the well-known correlations between particles generated by intermolecular forces in gas dynamics.

They considered a three dimensional classical system of two constituents: supersaturated solution and spherical second phase particles with stationary positions. Such a system has two characteristic lengths; the mean particle radius $\bar{R}(t)$, and The *screening length* $l \equiv 1/[4\pi n(r)\bar{R}(t)]^{1/2}$, where $n(t)$ is the number of particles per unit volume. It is assumed that the particle volume fraction $Q(t) \equiv [4\pi n(t)\bar{R}(t)^3/3]$ is small so that

$$\frac{\bar{R}(t)}{l(t)} = [3Q(t)]^{1/2} \ll 1 \tag{75}$$

Then, the change of the radius $R_i(t)$ of the i th particle or growth rate is given by

$$\frac{\partial R}{\partial t}\frac{4}{3}\pi R_i(t)^3 = -4\pi D M_i(t) \tag{76}$$

where

$$M_i(t) = R_i(t)\left[\frac{l_C}{R_i(t)} - \Delta(t)\right] - \sum_{j\neq i}^{N}\frac{M_j(t)}{|X_i - X_j|} \tag{77}$$

where D is the diffusion coefficient, l_C is the capillarity length (see Equation 2), N the number of second phase particles and X_i the position vector of the center of the i th particle. $\Delta(t)$ represents the degree of the supersaturation and its time evolution is determined by the conservation law as

$$\dot{q}(t) + \dot{\Delta}(t) = 0; \quad q(t) = \sum_{i=1}^{N}\left[4\pi R_i^3(t)/3V\right] \tag{78}$$

where V is the volume of the system and dots denote time derivatives. The first term of Equation 77 predicts that if $R_i > l_C/\Delta$, the particle grows and if $R_i < l_C/\Delta$, it dissolves, leading to a critical radius $R_o = l_C/\Delta$. The

second term on Equation 77 represents the cooperative effects among particles.

An advantage of the TK model is that in the thermodynamic limit, i.e., $N \to \infty$ and $V \to \infty$, $N/V \to$ constant, it is possible to explicitly evaluate the magnitude of the distribution functions of $f(R, t)$. In the TK model it was shown that there are two characteristic stages of coarsening, depending on their space-time scales; an *intermediate stage* and a *later stage*. In both stages, new equations were derived to order $Q^{1/2}$. These equations have two terms at order $Q^{1/2}$; a *collisionless drift term* and a *collision term*. It is also shown that in both stages that the mean particle radius increases as the cube root of the time ($t^{1/3}$). A scaling behavior of the distribution function $f(R, t)$ was observed to exist in both stages. Especially, in the late stage this scaling behavior was shown to coincide with that obtained by the LSW in the limit $Q \to 0$. In the intermediate stage during a first-order process where $Q = Q(t)$, the particle radius distribution is not time independent but does obey a scaling relationship and more importantly $\bar{R}$ is proportional to $t^{1/3}$. An experimental result [53] has shown that $\bar{R}$ is proportional to $t^{1/3}$ when $Q = Q(t)$ although the results are not completely convincing due to experimental error.

5.7. The VG theory (1984)

Voorhees and Glickman [13, 14] developed a theory describing the simultaneous growth and shirinkage of a randomly dispersed phase in a matrix, with the second phase providing the only sources or sinks of solute and/or heat, as is the case during Ostwald ripening. This theory provides a description of the interparticle diffusional interactions which occur during coarsening. Furtheremore, since the theory was developed in a form which permits the coarsening rates of large numbers of particles to be calculated, it is also possible to determine the influence of interparticle diffusional interactions on the collective behavior of a system of ripening particles. The theory is based on a quasi-steady-state approximation to the time-dependent diffusion equation, i.e. the multiparticle diffusion (MPD) solution (see Section 3.1) is based upon the time-dependent Laplace equation.

The MPD problem involves the simultaneous emission and absorption of diffusant at second phase domains distributed in a matrix. For the description of MPD as general as possible, the diffusion equation is expressed in terms of dimensionless variables (see Section 2.2). All space variables are nondimensionalized by a characteristic distance, l_C. The value of the diffusion field is denoted by $\theta(r)$, where in general, $\theta(r)$ can be a dimensionless pressure, temperature, solute concentration, etc depending on the problem.

A description of the slowly changing diffusion field in a medium consisting of N sources or sinks at fixed locations can be found by solving a form of Poisson's equation (see Section 3.1):

$$\nabla^2(\theta) = \sum_{i=1}^{N} -4\pi B_i \delta(r - r_i) \qquad \text{(see Equation 12)}$$

where θ is a dimensionless temperature or concentration (see Equation 4) r is a dimensionless vector locating the arbitrary field point, r_i is a dimensionless vector which locates the center of the ith particle, δ is a Dirac delta function, and B_i is a constant whose magnitude is a measure of the strength of the point source ($B_i > 0$) or sink ($B_i < 0$), N is the number of sources or sinks in the system. All quantities which have units of length are scaled by the capillary length l_C (see Equation 2).

$\theta(r)$ represents some scalar potential within the diffusing medium resulting from the contribution of N point sources and sinks. It is therefore possible to apply the methods of potential theory to simplify the problem. Therefore, $\theta(r)$ will be termed simply the potential, or dimensionless temperature or solute concentration as the case requires. A general solution to Equation 12 is the linear combination,

$$\theta(r) = B_o + \sum_{i=1}^{N} \frac{B_i}{|r - r_i|} \qquad \text{(see Equation 13)}$$

where B_o is some constant reference potential which, in general, is nonzero. Equation 13 indicates that each source and sink contributes to the total temperature/concentration field at a given point in the matrix.

In applying the VG theory to the multi-particle diffusion case the Ostwald ripening problem is solved using the diffusion field within the matrix:

$$\Delta^2\theta = -4\pi B_i \delta(r - r_i) \tag{79}$$

The location of the particles within both the translated and reference unit cells are specified by basis vectors of the type r_i and r_j which locate the centers of the ith and jth particles, respectively.

With the boundary conditions

$$\theta_j = -\frac{1}{R_j} \quad \text{for} j = 1, \ldots, N' \text{and} \tag{80}$$

$$\sum_{i=1}^{N} \dot{H}_i = 0 \tag{81}$$

where θ_j is the dimensionless interfacial potential for the jth particle of dimensionless radius R_j; $\dot{H}_i$ is the rate of dimensionless entalphy (or solute) loss or gain from the ith particle, where $H = H^*/l_C^3 L$ for the solid-liquid mixtures, $H = H^*\Omega/l_C$ for the solute diffusion case and H^* is a dimensional entalphy or solute content of a particle. L is the latent heat of fusion.

The better idea about coarsening can be gained by considering a two-particle case. The two-particle basis allows the problem to be solved analytically. For the VG model The following simplified two-particle kinetic equation can be written

$$\dot{R}_1 = R_1^{-2} \left[\frac{R_1 - R_2}{R_2 + R_1 + \dfrac{2R_1R_2}{a_o}(D_c - \vartheta_c)} \right] \tag{82}$$

where R_1 and R_2 are the dimensionless radii for the particles 1 and 2, respectively. $\dot{R}_1 = \mathrm{d}R_1/\mathrm{d}t$. The terms

D_C and ϑ_C are defined in bracketed expressions appearing in Equations 25 and 26 in [13]. D_c function represents the potential at the center of the jth particle arising from its image sources or sinks located in the displaced unit cell. The term D_c therefore represents the self-interaction of the j th particle with the lattice of its images. As a result D_c depends only on the Bravais lattice chosen to translate the basis, and for a given Bravais lattice, D_c is a constant independent of the particle basis. The ϑ_{ij} determines the magnitude of the interaction between the ith and jth particles. ϑ_c is a constant once the locations of the particles within the unit cell are chosen. Specifically both D_c and ϑ_{ij} terms vary as a_o^{-1} (a_o is the lattice parameter constant), and in the limit $a_o \to \infty$ the interaction terms vanish.

The concept of a "Madelung's constant" for a given Bravais lattice is applicable to the coarsening problem [19]. In the simple two-particle basis, the generalized Madelung's constant $M(\alpha_i, \beta_i, \gamma_i) = \vartheta_C - D_C$, where $\alpha_i, \beta_i, \gamma_i$ denote the components of the basis vector locating the ith particle. Thus, Equation 82 can be written in terms of a generalized Madelung's constant as

$$\dot{R}_1 = \frac{1}{R_1^2}\left[\frac{R_1 - R_2}{R_1 + R_2 - 2R_1R_2\dfrac{M(\alpha_i, \beta_i, \gamma_i)}{a_o}}\right] \quad (83)$$

It is possible to compare the coarsening rates predicted by Equation 83 to those predicted by the LSW theory. In the dimensionless form the LSW coarsening rates are defined by [23]

$$\dot{R}_1^{LWS} = \frac{1}{R_1}\left[\frac{1}{\bar{R}} - \frac{1}{R_1}\right] \quad (84)$$

where $\bar{R}$ is the average particle radius. If R_1 is larger than $\bar{R}$ then the particle will grow ($\dot{R}_1 > 0$), and if R_1 is less than $\bar{R}$, then the particle will shrink ($\dot{R}_1 < 0$). The LSW coarsening rates can be compared with the "two-particle" coarsening rates predicted by a two-term expansion of Equation 83, namely

$$\dot{R}_1 = \frac{1}{R_1^2}\left[\frac{R_1 - R_2}{R_1 + R_2}\left\{1 + \frac{2R_1R_2}{(R_1 + R_2)a_o M} + \left(\frac{2R_1R_2}{(R_1 + R_2)a_o}M\right)^2 + \cdots H.O.T.\right\}\right] \quad (85)$$

The relative difference in the coarsening rates predicted with Equation 85 from the LSW coarsening rates is to first order

$$\frac{\dot{R}_1 - \dot{R}_1^{LSW}}{\dot{R}_1^{LSW}} \cong \frac{2R_2R_1M}{(R_1 + R_2)a_o} \quad (86)$$

For any given particle arrangement in the unit cell, as $a_o \to \infty$ (implaying that the volume fraction vanishes) the RHS of Equation 86 also approches zero. This result is consistent with the fact that the LSW theory is valid only in the asymptotic limit of zero volume fraction. It is also interesting to point out in Equation 86 that if the radius of ith particle approaches zero, then the LSW coarsening rates are again recaptured. This implies that the coarsening rates of small particles (on the dimensionless length scale) are not strongly influnced by neighboring particles, even though the distance between the particle centers might itself be small. A final point here is that $M(\alpha_i, \beta_i, \gamma_i) > 0$, implying that the coarsening rate of either particle is always faster than that predicted by LSW.

In conclusion, the VG theory is consistent with the LSW theory at zero volume fraction, and at the higher volume fractions an analysis carried out on a two-particle basis indicates an increase in the coarsening rates of both particles. The coarsening rates of small particles are not expected to be affected strongly by diffusional interactions. Small particles should coarsen at rates close to those predicted by the LSW theory, even at high volume fractions.

5.7.1. Comparisons of The VG theory with MLSW, LSEM and BW theories

As discussed in previous sections, the theories of MLSW, BW, and LSEM predict the steady-state distributions at non-zero volume fraction. A precise comparison between the theories of LSEM, BW and the VG is possible at a volume fraction of 0.1. The overall functional forms of the distributions are similar. All three predict a steady-state distribution which is broader, less peaked, and more symmetric than LSW. However, there are differences between each of the predicted curves. The VG theory appears to predict a distribution with a greater peak height than those of BW or LSEM. However, The VG theory agrees with the BW theory on the location of the foot of the probability distribution at the high-ρ end and disagrees with LSEM. At higher volume fractions direct comparisons are not possible; however, it appears that the VG predicts a broader distribution with a lower peak height than LSEM and BW. Generally, the VG theory predicts steady-state distributions which are more peaked at low volume fractions, and which are broader at high volume fractions than those predicted by LSEM and BW. For the comparison of these theories, the dependence of the rate constant on the volume fraction is established in Fig. 11; in this figure the rate constants predicted by the theories of Ardell (MLSW), BW, LSEM, and GV are shown as a function of the volume fraction. The rapid increase in K predicted by the MLSW model is based upon an unrealistic statistically averaged rate constant. The curve for the LSEM is lower than the VG which is attributable to the improper assumption used by the theory [13]. The VG theory indicates that coarsening rates are noticeably different from the LSW predicted coarsening rates even at volume fractions as low as 0.05. It is therefore unlikely that the rate constants predicted by the LSEM can be applied at non-zero volume fraction. In the range $0 < Q < 0.35$ the VG and BW theories predict rate constants which differ by 50%, with the BW theory predicting a higher sensitivity of the rate constant on volume fraction. A second major difference between these two theories is the predicted functionality of the rate constant with volume fraction in the range

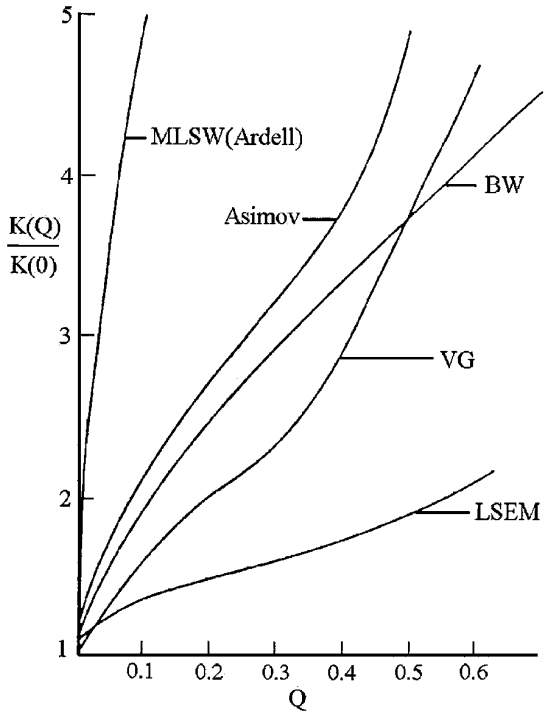

Figure 11 The VG rate constant ratio $K(Q)/K(0)$ versus the volume fraction Q. For comparison LSW, LSEM, BW, and MLSW curves are also included [14].

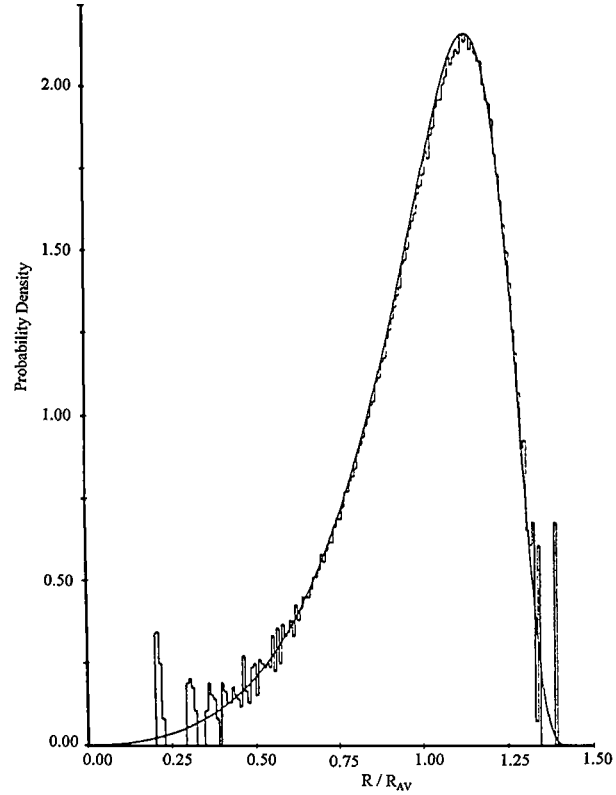

Figure 12 Steady-state analytical distribution from LSW theory and simulation derived histogram at $Q = 0$ for the VG model. General agreement is satisfactory; noise in histogram near the tails of the distribution occur because of the finite number of basis particles used in the simulation [14].

$Q > 0.35$, where the VG theory indicates that the rate constant is a more sensitive function of volume fraction than the almost linear form of the BW theory.

5.7.2. Computer simulations for the multiparticle diffusion (MDP) problem: application of computer simulations on the VG theory

A critical test of the numerical approach for the VG theory was made [14] by comparing the coarsening simulation in the limit of zero volume fraction to the analytic results of the LSW theory. Since the LSW theory employs a continuum statistical mechanical approach, the theory makes specific analytic predictions on the collective behavior of coarsening systems. In contrast, the VG theory employs a discrete approach to determine the diffusion field within a coarsening medium, and then uses the computer to investigate the collective behavior of the system. Therefore, the LSW theory provides an important test for establishing the simulation's ability to model the behavior of coarsening systems. In this simulation work, the statistical properties which are examined include:

(i) the growth of the cube of the average particle radius; the LSW theory predicts the following functional form

$$\bar{R}^3(t) - \bar{R}^3(0) = K(0)t$$

where $\bar{R}(t)$ is the average radius at time t, $\bar{R}(0)$ is the average particle radius at time $t = 0$, K is the rate constant, the value of which at $Q = 0$ is 4/9, and

(ii) the appearance of a unique time-invariant particle radii distribution when the particle radii are plotted in terms of $\rho = R/\bar{R}$. In this calculation the volume fraction of phase was set equal zero. The steady-state histograms for the VG theory, along with the analytic LSW distribution, is shown in Fig. 12. There is a little difference between the computed steady-state histogram and the distribution predicted analytically by LSW.

The local particle environment is responsible for the hills and valleys of $\bar{R}^3$ plot over many time-steps. The peaks of the steady-state histograms are associated with the influence of particle interactions on the particle trajectories in ρ-space. This explains the relative smoothness of the LSW steady-state histogram shown in Fig. 12.

Fig. 13 shows the cube of the average particle size vs time. The growth rate of the cube of the average particle radius is linear in time, and the regressed rate constant is 0.4397, which is within 1.0% of the 0.4444($\cong 4/9$) slope predicted by the LSW theory.

The dependence of the rate constant, K, on volume fraction is illustrated in Fig. 14, where $K(0) = 4/9$ is rate constant of LSW. The small particle interactions at the lower volume fractions resulted in small standard deviations of the rate constant. Also evident is the factor-of-four increase in the rate constant resulting from an increase in the volume fraction from 0 to 0.5. Hence, it is concluded that the enhanced diffusional interactions which occur at finite volume fractions result in larger rate constants for the coarsening system than under conditions appropriate to the LSW theory.

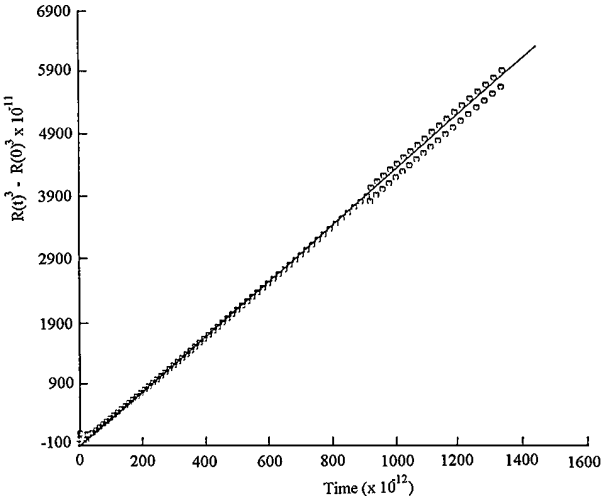

Figure 13 Cube of the average particle size versus time with $Q = 0$. The theory line indicates slope of 4/9, which agrees closely with simulation data) [14].

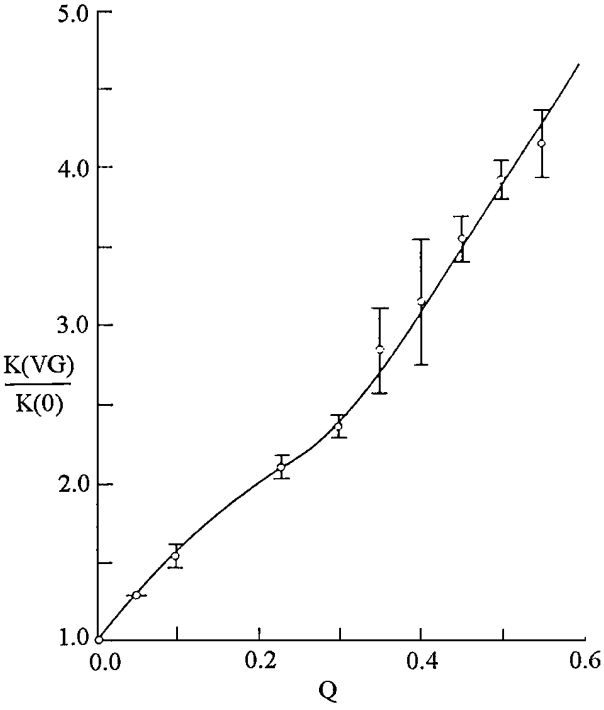

Figure 14 The rate constant ratio, $K(Q)/K(0)$, versus Q, where $K(Q)/K(0)$ is the VG simulation result divided by LSW rate constant $K(0)$. The error bars were computed as the standard deviation. This figure also illustrates that there will be a significant increase in the coarsening rate of the mixture as Q increases [14].

Fig. 15 shows the steady-state distributions at various volume fractions. This figure shows that interparticle diffusional interactions play a major role in determining the form of the steady-state distribution at a given Q.

5.8. The ETK theory (1986)

Enomoto *et al.* [23] (the ETK theory) investigated the effect of a finite volume fraction of precipitate particles on the Ostwald ripening on the basis of a statistical theory. This theory takes into account both the competitive growth and so-called soft-collision effect of particles arising from statistical correlations among

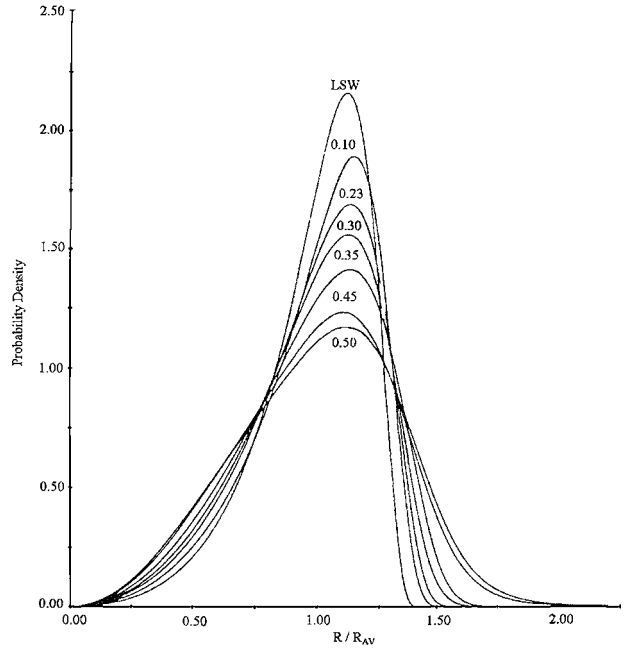

Figure 15 VG steady-state distribution at various volume fraction Q. This figure shows that interparticle diffusional interactions play a major role in determining this distribution at a given Q [14].

them because the soft-collision processes are important in coarsening as anticipated by the TK theory [24]. In this theory a second-order differential equation for the single particle distribution function obtained from a Fokker-Planck type equation was used numerically and stress the importance of the soft-collision process in ripening.

Let $p(\rho)$ denote the relative particle size distribution function with $\rho \equiv R/\bar{R}(t)$, where R is the particle radius and $\bar{R}(t)$ its average. $p(\rho)$ then obeys the following second-order differential equation, to order $\sqrt{Q}$

$$\left(4 + \rho\frac{\mathrm{d}}{\mathrm{d}p}\right)p(\rho) = (3l_C D/K)x\left[B(\rho) - \sqrt{3Q/m_3}\frac{\mathrm{d}}{\mathrm{d}p}E(\rho)\right]p(\rho) \tag{87}$$

and

$$\bar{R}^3(t) - \bar{R}^3(0) = K(Q)t \qquad \text{(see Equation 32)}$$

where K is a coarsening rate given by

$$K = l_C D \operatorname*{Lim}_{p\to 0} p(\rho)/\rho^2 \tag{88}$$

Here D is the diffusion coefficient, l_C the capillarity length and m_n the n th moments defined by

$$m_n = \langle \rho^n \rangle = \int \rho^n p(\rho)\,\mathrm{d}\rho \tag{89}$$

The averaged source/sink strength $B(\rho)$ is given by

$$B(\rho) = -\lambda(\rho) - \sqrt{3Q/m_3}[v(\rho) + c(\rho)] \tag{90}$$

with collisionless drift terms

$$\lambda(\rho) = 1 - \rho \tag{91}$$

$$v(\rho) = \rho(m_2 - \rho) \tag{92}$$

and the soft-collision term

$$c(\rho) = \mathrm{d}(\rho) - \langle \mathrm{d}(\rho) \rangle \rho \tag{93}$$

$$\mathrm{d}(\rho) = \rho\lambda(\rho)\left[\sqrt{1+a_+} - 1\right] - \frac{\mathrm{d}E(\rho)}{\mathrm{d}(\rho)} - E(p)/\rho \tag{94}$$

where the kinetic coefficient $E(\rho)$ is given by

$$E(\rho) = \begin{cases} \left[(b_+ + a_+ b_-/a_-)\left(1 - \sqrt{1-a_-}\right)\right] \\ \quad + (b_+ - b_-)\left(\sqrt{1+a_+} - 1\right) \\ \quad \times (a_+ + a_-), \quad \text{if } a_- \le 1 \\ [b_+ + a_+ b_-/a_+ + (b_+ - b_-)] \\ \quad \times \left(\sqrt{1+a_+} - 1\right) \end{cases} \tag{95}$$

Here $a_\mp$ and $b_\pm$ are functions of ρ defined by Equations 1.12 and 1.13 in [17]. The effect of the collisionless drift processes is analyzed below, to order $\sqrt{Q}$ The coarsening rate $K(Q)$ for the collisionless drift processes is given by

$$K(Q) = 3l_C D\left(1 + \sqrt{3Q/m_3}\rho_c^2\right)/2\rho_c^3 \tag{96}$$

where ρ_c is a cut-off, and is given by a solution of the equation

$$\rho_c - 3 + \sqrt{3Q/m_3}\rho_c(\rho_c - 2m_2) = 0 \tag{97}$$

The relative particle size distribution $p(\rho)$ is

$$p(\rho) = \begin{cases} N\rho^2(\rho_c - \rho)^{-a}(\rho_o + \rho)^{-b} \\ \quad \times \exp[-c/(\rho_o - \rho)] & \rho < \rho_c \\ 0, & \rho \ge \rho_c \end{cases} \tag{98}$$

Here

$$\rho_o = 3l_C D/\left(K\rho_c^2\right) \tag{99}$$

where

$$\begin{aligned} a &= 2 + 3\rho_c(\rho_c + 2\rho_o)/(\rho_c + \rho_o)^2 \\ b &= 1 + 3\rho_o^2/(\rho_c + \rho_o)^2 \\ c &= 3\rho_c^2/(\rho_c + \rho_o) \end{aligned} \tag{100}$$

and N is the normalization constant determined by [17] as

$$N = 3\rho_c^{a-2}\rho_o^{b-1}\exp(c/\rho_c) \tag{101}$$

The relative size distribution function $p(\rho)$ is calculted from Equations 98, 96, 97 and 99 by using iterating m_2 and m_3 values. Using this iterative approach Enomoto *et al.* [17] found that in the dilute limit $Q \to 0$, $3l_C D/K = 27/4$ and $\rho_c = 3/2$ from Equation 96 and 97. Since these values are the same as those found in the LSW theory, the distribution function (Equation 98) reduces to that obtained by LSW.

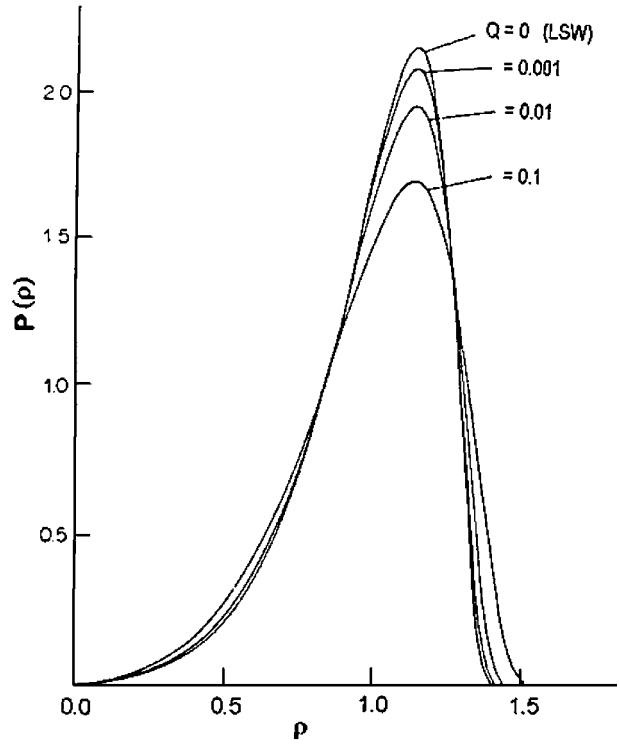

Figure 16 The ETK distribution function $p(\rho)$ with only drift process at $Q = 0.001, 0.01, 0.1$. LSW result is also included for comparison [17].

5.8.1. Comparison of the ETK model with the LSW, BW, MR, TK and MLSW theories

Fig. 16 shows the normalized scaled particle size distribution function $p(\rho)$ (with only the drift process) against ρ for a series of different volume fraction Q (i.e. for $Q = 0.001, 0.01, 0.1$). The effect of Q-dependence collisionless drift processes, $\sqrt{3Q/m_3}\ v(\rho)$ in Equation 90, are to lower and to broaden the peak of $p(\rho)$ as compared with that of the LSW theory. Fig. 17 shows the particle size distribution functions for the ETK theory at $Q = 0.1$ and $Q = 0.35$, respectively, which are compared with the results obtained in other theories and in the LSW theory. These theories except the Ardell theory and the LSW theory are in fair agreement with each other for small Q. However, as the volume fraction Q increases, differences appear gradually among these theories.

Fig. 18 illustrates the reduced coarsening rate $K(Q)/K(0)$ variation against the volume fraction Q. Those obtained by Ardell (MLSW), BW, MR, and VG are also shown for comparison. In this figure, VG(D) means the result given by the VG effective medium theory (see Section 4.6) and the data bars are from the computer simulation data [54]. The ETK results with the soft-collision effects included is indicated by ETK $(d + S)$. The ETK result in which the collisionless drift processes are taken into acount is also displayed as ETK(d) for comparison with other theories. All the results agree up to $Q \cong 0.1$ except those of Ardell and BW. Beyond $Q \sim 0.1$, ETK $(d + S)$ starts to deviate from

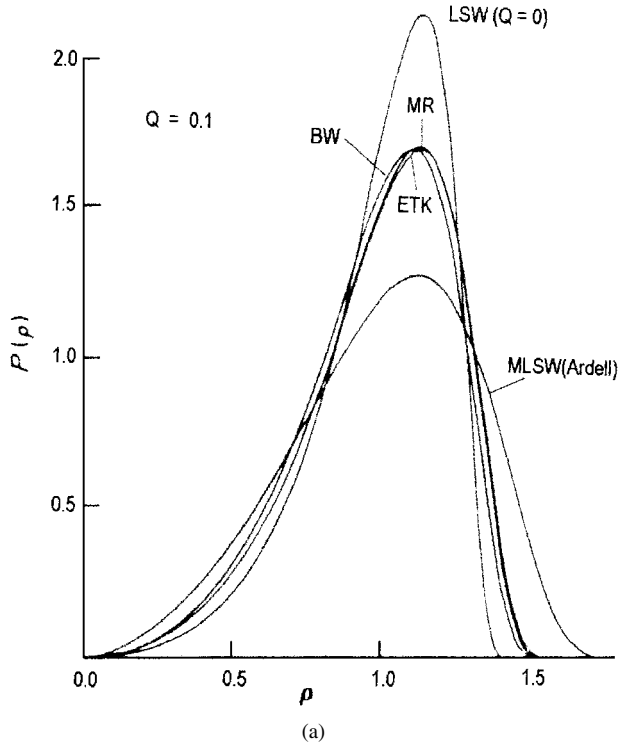

(a)

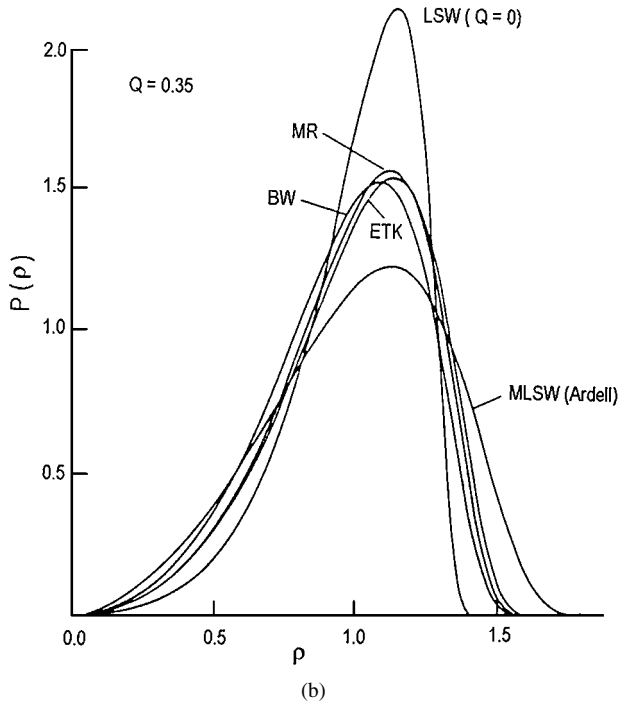

(b)

Figure 17 The ETK distribution functions $p(\rho)$ at various volume fractions Q. The results from other theories are also included [17]. (a) $Q = 0.1$ (b) $Q = 0.35$.

ETK (d). This agrees with the prediction of the VG simulation [26] that the spatial correlations begin to build up at $Q \sim 0.1$. Here we should remark that for $Q > 0.2$, there is a disagreement between ETK ($d + S$) and the result of the VG effective medium theory [VG(d)], although the distribution function $p(\rho)$ of both theories are in good agreement at $Q = 0.35$.

Enomoto *et al.* [17] have also investigated the effects of both the drift and soft-collision processes. The soft-collision terms are of the order $\sqrt{Q}$, and hence the effects on $p(\rho)$ and $K(Q)$ due to them are of the same order as the drift contributions. The asymptotic solution

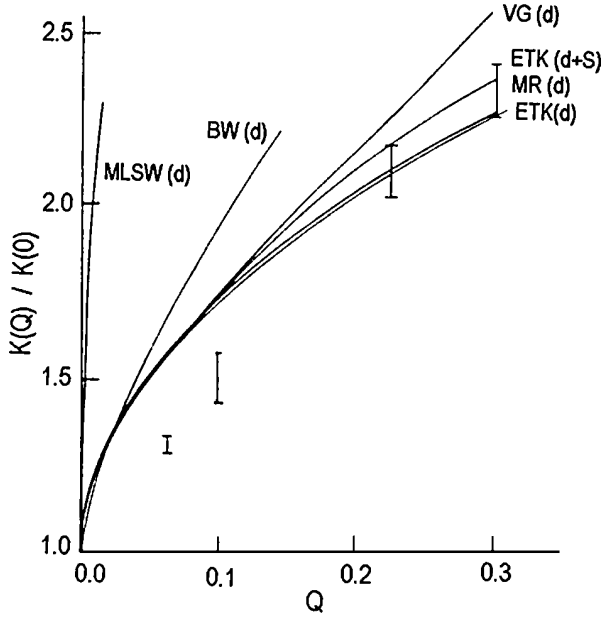

Figure 18 Plots of the relative coarsening rates $K(Q)/K(0)$ in the ETK model. Here (d) indicates the result with only the drift process and $(d + S)$ with both drift and soft-collision processes. The bars indicate the typical scatters in the computer simulation data by VG [17].

for the relative size distribution function $p(\rho)$ for both the effect of the drift and soft-collision processes is

$$p(\rho) \sim \rho \exp\left(-\frac{\rho^4}{4\varepsilon E}\right) \quad \text{for large } p. \tag{102}$$

where

$$\varepsilon = (3l_C D/K)\sqrt{3Q/m_3} \tag{103}$$

In Figs 19–21 the particle size distribution function involving both drift and soft-collision processes are

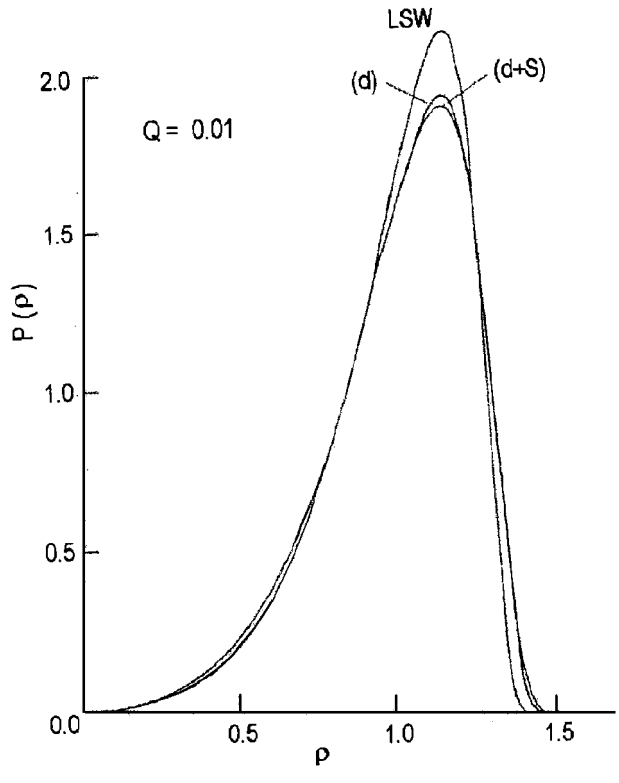

Figure 19 Plots of the ETK distribution function $p(\rho)$ at $Q = 0.01$ [17].

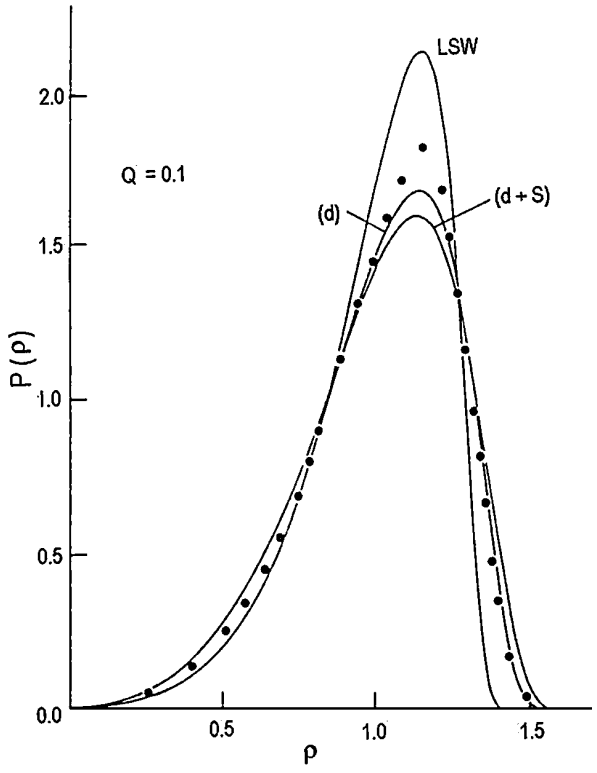

Figure 20 Plots of the ETK distribution functions $p(\rho)$ at $Q = 0.1$. The dots exhibit the results of the VG computer simulation [17].

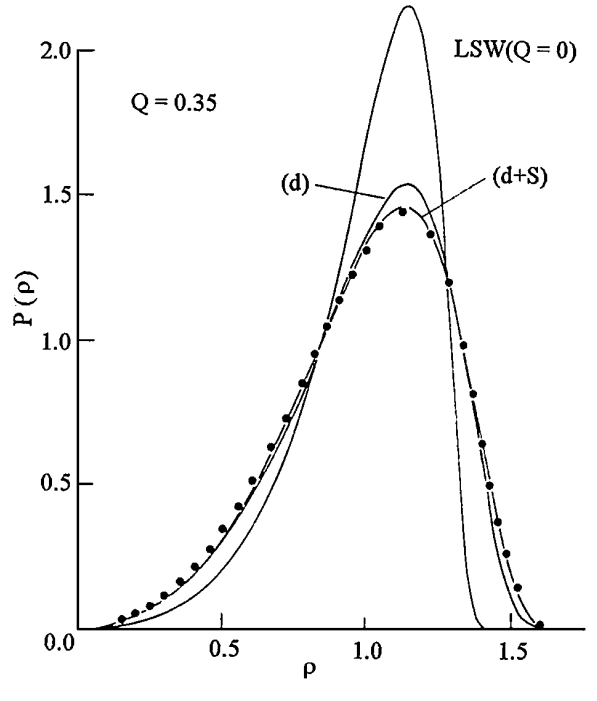

Figure 21 Plots of the ETK distribution functions $p(\rho)$ at $Q = 0.35$. The dots are results of the VG computer simulation [17].

plotted at three different values of the volume fraction $Q = 0.01$, 0.1 and 0.35, respectively, and are compared with the LSW results and the ETK results that include only the drift processes at the same values of the volume fraction. In Figs 20 and 21 the dots represent the computer simulation results by VG. From these we can say that the effects of both processes on $p(\rho)$ lead to further flattening and broadening of the distribution function so as to lower the peak and to shift it slightly to the left. In Fig. 20 the VG distribution function with $Q = 0.1$ is not in agreement with the other theories especially near $\rho = 1$, although agreement with the ETK theory is better for large and small ρ. However, in Fig. 21 $p(\rho)$ for the VG theory at $Q = 0.35$ is in good agreement with the ETK that includes both the drift and the soft-collision processes.

5.9. The YEGG theory (a mean-field theory) (1993)

Yao *et al.* [15] have made a thoretical approach to the Ostwald ripening of precipitate particles in dimension $d \geq 2$. A mean-field theory was constructed to incorporate screening effects in the competing-particle system. The mean-field equations were solved to infinite order in the volume fraction and provide analytic expressions for the coarsening rate, the time-dependent particle-distribution function, and the time evolution of the total number of particles.

In this study the dimensionless variables are used (see Section 2.2). Units of length and time are given in terms of a characteristic length

$$l_C = \frac{(d-1)\gamma\Omega}{R_B T}$$

and a characteristic time

$$t^* = \frac{l_C^2}{dC_e\Omega}$$

It is also convenient to introduce a dimensionless concentration field

$$\theta(r) = \frac{C(r) - C_\infty}{C_\infty}$$

All the quantities involved here have been defined in Section 2.2.

The many-particle diffusion problem is intractable without approximation. In the steady-state limit, the fundamental Equation [13, 14, 26] (see Section 3.1) is

$$\nabla^2\theta(r) = \varphi \sum^{N} B_i(r - r_i) \qquad (104)$$

where N is the number of the particles in the system, $\varphi = 2\pi^{d/2}/\Gamma(d/2)$, r_i gives the location of the ith particle, and B_i is the strength of the source or sink of current for diffusion. This is the multiparticle diffusion (MPD) equation in the quasistationary approximation, where $\partial\theta/\partial t$ is neglected because the growth rate of particles is much slower than the relaxation time of concentration field in the matrix. The necessary boundary conditions are the Gibbs-Thomson condition (Section 2.1) for the concentration field at the curved surface of each particle and the imposed supersaturation far from all particles:

$$\theta(r)|_{|r-r_i|=R_i} = \frac{1}{R_i} \quad \text{and} \quad \lim_{r\to\infty} \theta(r) = \theta_{\text{av}} \qquad (105)$$

for $i = 1, \ldots, N$, where θ_{av} is the average concentration outside the particles. The conservation law is

$$\sum_{i=1}^{N} B_i = 0 \qquad (106)$$

which implies that the limit in which the minority phase (within the particles) and majority phase (outside the particles) are at their equilibrium concentration (see Section 3.1), and the growth law satisfies

$$\frac{\mathrm{d}\left(v R_i^d\right)}{\mathrm{d}t} = -\int_{s_i} J \cdot n \, \mathrm{d}\sigma \tag{107}$$

where s_i is surface of the ith particle, n is the unit vector normal to the particle surface, and $v = \pi^{d/2}/\Gamma(d/2+1)$. Substituting the Fourier-Fick law $J = -\nabla\theta$ into Equation 107 and transforming the surface integral over the ith particle into a volume integral gives

$$\frac{\mathrm{d}\left(v R_i^d\right)}{\mathrm{d}t} = \int \nabla^2\theta \, \mathrm{d}v \tag{108}$$

The explicit form of the growth law can then be obtained by substituting Equation 104 in Equation 108, i.e.,

$$\frac{\mathrm{d}R_i}{\mathrm{d}t} = \frac{B_i}{R_i^{\mathrm{d}}} \tag{109}$$

LSW made a mean-field approximation in the limit of $Q \to 0$ to solve these equations. For nonzero Q the steady-state problem resembles a homogeneous electron gas since particles interact via the Laplace equation in the steady-state limit and charge neutrality is invoked through Equation 106. Here screening effects are introduced among the particles and approximate the many-particle correlation effects in the same manner as the Thomas-Fermi mechanism for Coulomb systems. Within a mean-field approximation, the change in volume of a particle only depends on the concentration gradients set up by each particle.

To compare with other theories and experiments The YEGG model has given the scaled distribution function using the conventional scale variable $z = R/\bar{R}$ as

$$g(z) = x_{\mathrm{av}} G(x_{\mathrm{av}} z), \text{ i.e.,}$$

$$g(z) = \begin{cases} \dfrac{-\mathrm{d}\lambda x_{\mathrm{av}}}{\omega(x_{\mathrm{av}} z, \lambda)} \exp\left[\mathrm{d}\lambda \displaystyle\int_0^{x_{\mathrm{av}} z} w^{-1}(z', \lambda)\, \mathrm{d}z'\right] \\ \qquad\qquad \text{if} \quad 0 < z < z_{\mathrm{o}} \\ 0 \qquad\qquad \text{otherwise} \end{cases} \tag{110}$$

where $z_{\mathrm{o}} = x_{\mathrm{o}}/x_{\mathrm{av}}$ and $x_{\mathrm{av}} = \int_0^\infty x G(x)\mathrm{d}x$. The procedure for defining various functions and quantities such as x_{o}, λ, z', z in Equation 110 are given in [15].

The average radius of the particles, $\bar{R}(t)$, and the total number of the particles, $N(t)$, can now be calculated. From the definition given in [21], $\bar{R}(t)$ becomes

$$\bar{R}(t) = [\bar{R}(0) + K'(Q)t]^{1/3} \tag{111}$$

where $K'(Q) = 3\lambda x_{\mathrm{av}}^3$. Equation 111 indicates that the coarsening exponent is universal and dimension independent. For $Q \to 0$ in $d = 3$, Equation 111 becomes

$$\bar{R}(t) = [\bar{R}^3(0) + 4t/9]^{1/3}$$

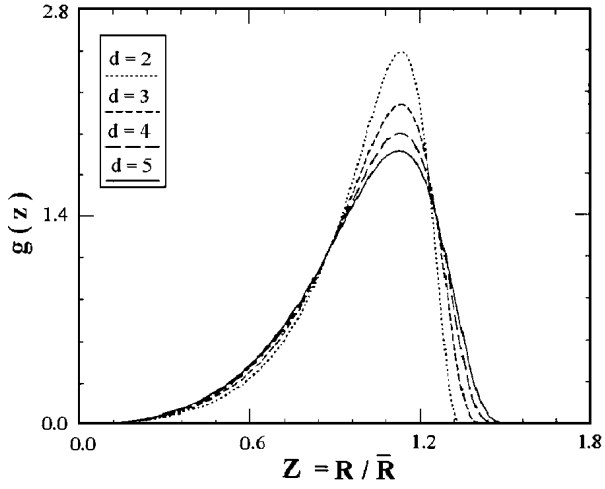

Figure 22 Comparison [15] of the YEGG scaled normalized distribution functions $g(z)$ for the YEGG model versus scaled particle radius $z = R/\bar{R}$ for $Q \to 0$ in $d = 2$, 3, 4, and 5.

(see Equation 30a), recovering the LSW result. Finally, the time evolution of the number of the particles for the YEGG model is given by

$$N(t) = \int f(R, t)\, \mathrm{d}R = \frac{N(0)\bar{R}^d(0)}{[\bar{R}^3(0) + K(Q)t]^{d/3}} \tag{112}$$

Fig. 22 shows the particle-distribution function for $Q \to 0$ in $d = 2$, 3, 4 and 5, which indicates that, in the limit $Q \to 0$, a higher-dimensional distribution function is broader than a lower-dimensional one. In this limit, except $d = 2$, the growth rate becomes

$$\frac{\mathrm{d}R}{\mathrm{d}t} = \frac{1}{R}\left[\frac{x_{\mathrm{av}}}{\bar{R}} - \frac{1}{R}\right] \tag{113}$$

x_{av} is a monotonically decreasing function of dimensions d; therefore, the critical radius $R^* = \bar{R}/x_{\mathrm{av}}$ increases with dimensions d. As a result, more particles shrink and less particles grow in higher dimensions than in lower dimensions. The growing particles in higher dimensions grow faster than those in lower dimensions on average, which results in a broader range distribution function for higher dimensions.

Fig. 23 presents the finite-volume-fraction effects on the YEGG scaled normalized distribution function (Equation 110) for $d = 3$. It indicates that the distribution function is sensitive to Q. As Q increases, $g(z, Q)$ becomes broader. In three dimensions, the growth law becomes

$$\frac{\mathrm{d}R}{\mathrm{d}t} = \frac{\exp(R/\xi)}{R}\left(\frac{\sigma}{u(t)} - \frac{1}{R}\right) \tag{114}$$

where u is arbitrary function of t in the scaling ansatz $f(R, t) = H(t)G[R/u(t)]$.

According to the numerical calculations, the *screening length* obeys $\xi \sim \bar{R}/\sqrt{3Q}$, and the critical radius $R^* = u(t)/\sigma$ is insensitive to the volume fraction Q, compared to $\exp(R/\xi)$, where σ is defined in [15]. Consequently, as Q increases, the particles whose radii are greater than the critical radius grow faster, and the particles whose radii are smaller than the critical

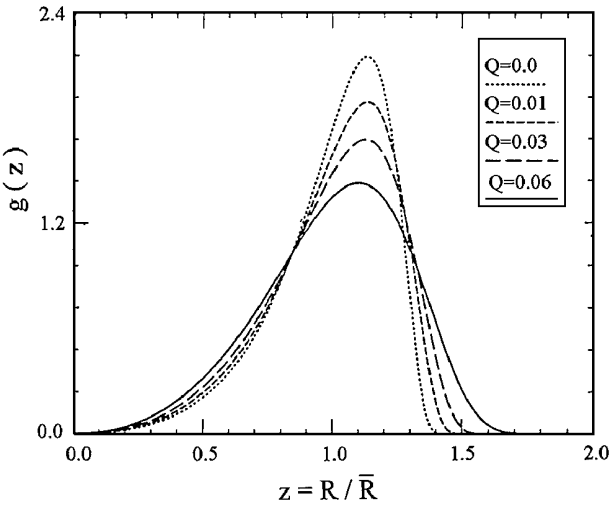

Figure 23 Predictions of the YEGG theory [15] for the scaled normalized distribution $g(z)$ versus scaled particle radius $z = R/\bar{R}$ are displayed for different Q for the dimension $d = 3$.

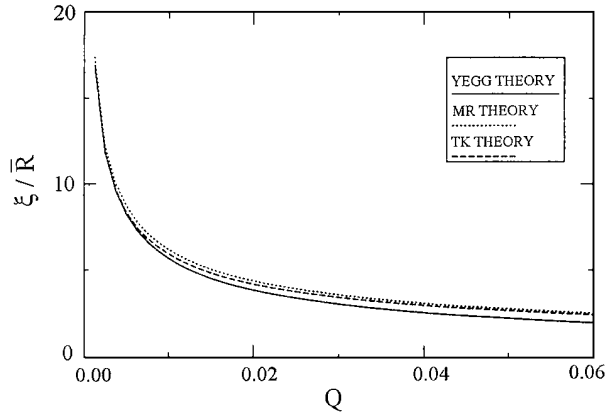

Figure 24 The scaled screening length $\xi/\bar{R}$ is displayed [15] as a function of Q. The dotted, dashed and solid lines correspond to the results of MR, ETK, and YEGG, respectively, in $d = 2$.

radius shrink faster, which leads to a broader particle distribution.

Fig. 24 displays the relation between the scaled screening length and the volume fraction: In $d = 2$, the scaled screening length for the YEGG versus the volume fraction is almost the same as the MR model's; in $d = 3$, the present model is close to that of both MR and TKE.

5.9.1. Basic equation for numerical simulations

To test mean-field theory results of discussed in the previous section, the numerical simulation similar to that of the VG theory [14] (see Section 5.7) have been used for the YEGG model. To derive the basic equations for this simulation, let us start from the solution of Equation 104 in three dimensions, i.e.,

$$\theta(r) = B_{\mathrm{o}} - \sum \frac{B_i}{|r - r_i|} \tag{115}$$

where B_{o} is an integration constant which, in general, is nonzero.

The Gibbs-Thomson boundary condition then becomes

$$\frac{1}{R_i} = B_{\mathrm{o}} - \sum_{i=1}^{N} \frac{B_i}{|r_i - R_j|} \tag{116}$$

where R_j is a position vector of the jth particle's boundary, and $R_j = |R_j - r_j|$ is the jth particle's radius. Using a monopolar approximation Equation 116 becomes

$$\frac{1}{R_j} = B_{\mathrm{o}} - \frac{B_j}{R_j} - \sum_{i=1, i\neq j}^{N} \frac{B_i}{|r_j - r_i|} \tag{117}$$

This monopolar approximation (Equation 117) was also adopted by the VG model [13, 14] (see Section 5.7) but in a different form. The relative difference between the growth rates $\{B_i\}$ for the present model and the VG work in their simulations is negligable. Therefore, the basic equtions for the present model are believed to be essentially the same as those of VG [15]. Similarly, the solution of Equation 104 in two dimensions is

$$\theta(r) = B_{\mathrm{o}} + \sum_{i=0}^{N} B_i \ln|r - r_i| \tag{118}$$

The Gibbs-Thomson boundary condition then becomes

$$\frac{1}{R_j} = B_{\mathrm{o}} + B_j \ln|R_j - r_j| + \sum_{i=1, i\neq j} B_i \ln|R_j - r_i| \tag{119}$$

Using the monopolar approximation for three dimensions Equation 119 can be written as

$$\frac{1}{R_j} = B_{\mathrm{o}} + B_j \ln R_j + \sum_{i=1, i\neq j}^{N} B_i \ln|r_j - r_i| \tag{120}$$

To provide equations suitable for numerical simulation in two dimensions, some manupilations of the fundamental equations are needed. To do so, let us split θ into two pieces, i.e., $\theta = \theta_1 + \theta_2$, θ_1 and θ_2 are solutions of the following equations:

$$\nabla^2\theta_1(r) = -2\pi\rho_1(r) \tag{121}$$

and

$$\nabla^2\theta_2(r) = -2\pi\rho_2(r) \tag{122}$$

Using the techniques developed by Voorhees and Glicksman [13–15] Equations 121 and 122 can be combined in the following way:

$$\theta(r) = B_{\mathrm{o}} - \frac{1}{2\pi}\sum_{i=1}^{N} B_i \int \frac{\mathrm{e}^{-\frac{k^2}{4\eta}}}{k^2}\,\mathrm{e}^{ik\cdot(r_i - r)}\,\mathrm{d}k - \sum B_i \int_{|r-r_i|}^{\infty} \frac{\mathrm{e}^{-\eta r'}}{r'}\,\mathrm{d}r' \tag{123}$$

where η is a positive constant.

A tractable form of Equation 120 can then be found using Equations 118, 123, and 120:

$$\frac{1}{R_j} = B_o + B_j\left[\ln(R_j/L) + \int_0^1 \frac{1-e^{-r'^2}}{r'}\,dr' - \int \frac{e^{-r'^2}}{r'}\,dr'\right] - \int \frac{e^{-r'^2}}{r'}\,dr'\Bigg] - \sum B_i \int_{|r_j-r_i|/L}^{\infty} \frac{e^{-r'^2}}{r'}\,dr' - \frac{2\pi}{L^2}\sum_{i=1}^{N} B_i \sum_{k\neq 0} \frac{e^{-k^2/4L^2}}{k^2} e^{ik\cdot(r_i-r_j)} \qquad (124)$$

where L is the system size. The basic equations used to simulate two-dimensional Ostwald ripening are the conservation law Equation 106, 124, and the two-dimensional version of Equation 114.

5.9.2. Results of numerical simulation

The most-time consuming step in the simulation is the calculation of the growth rates $\{B_i\}$, which is computationally of order N^3 (except for $d=3$ with $Q=0$). The present approach is essentially the same as that of VG (see Section 5.7).

To perform large-scale simulation it was started with 50,000 particles and then iterated until the number of particles was reduced to 25,000. In each iteration, only one particle was shrunk. The scaled distribution function, the time evolutions of both the average particle radius and the total number of particles have been plotted in Figs 25–27, respectively. In Fig. 25, the solid line is Equation 110 for $d=3$ and $Q\to 0$; the different symbols correspond to different times. All the symbols lying on the same universal solid line confirm the scaling behaviour of distribution function. Figs 26 and 27 show that the present numerical results give $\bar{R}(t)=[\bar{R}^3(0)+K'(Q)t]^{1/3}$ and $N(t)=N(0)\bar{R}^3(0)/[\bar{R}^3(0)+K'(Q)t]$, respectively, which are the same as Equations 111 and 112. From Figs 26 and 27, the values for $K(0)=0.4442$ and $K(0)=0.4434$ were obtained, from R and N, respectively. The relative difference between these independent measurements is about 0.2%. Comparing to the theoretical result, $4/9\cong 0.4444$, the relative difference is less than 0.3%, quite better than that of the VG simulations carried out on small systems [13, 14, 26] (see Section 5.7.).

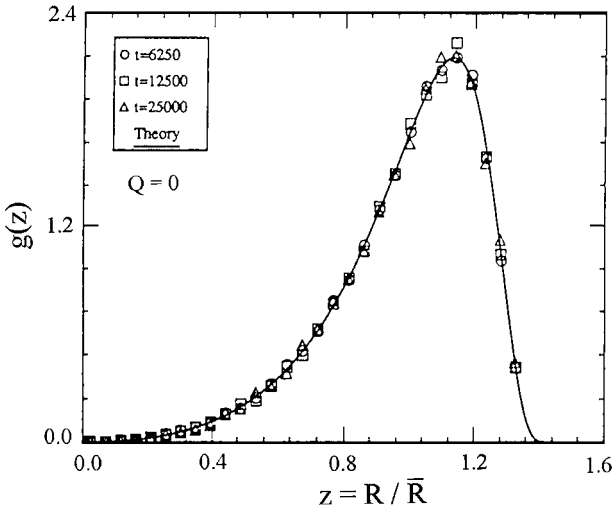

Figure 25 Predictions of the YEGG numerical simulation [15] for scaled normalized distribution $g(z)$ versus scaled particle radius $z=R/\bar{R}$, in $d=3$ and $Q\to 0$.

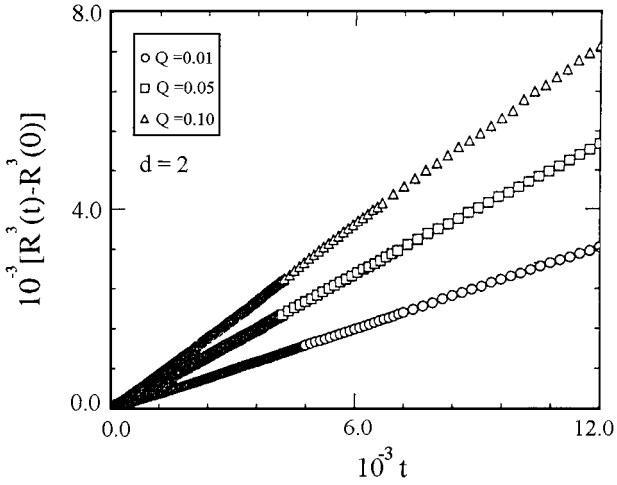

Figure 26 Results of numerical simulations for the time evolution of the average particle size $[\bar{R}^3(t)-\bar{R}^3(0)$ versus $t]$ for $Q=0.1$, 0.05 and 0.10 in $d=2$, for the YEGG [15]. The straight line indicates the time evolution of the average particle radius obeys $\bar{R}(t)=[\bar{R}^3(t)-\bar{R}^3(0)]^{1/3}$.

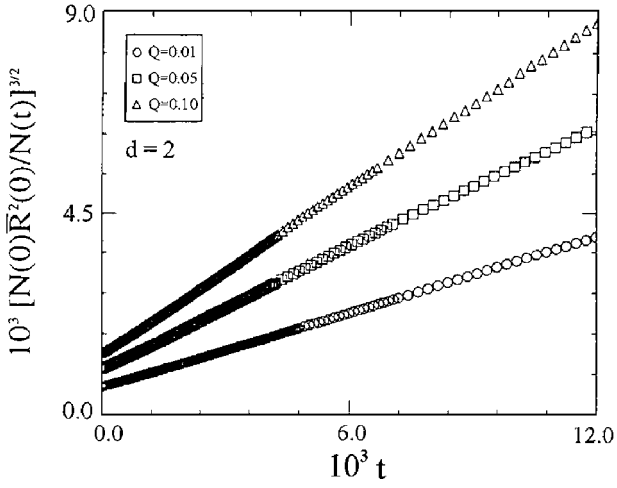

Figure 27 Plot for $[N(0)\bar{R}^d(0)/N(t)^{3/d}]$ versus t for $Q=0$, 0.05 and 0.10, in $d=2$, for the YEGG model [15]. The straight lines indicate that the time evolution of the number of the particles satisfies $N(t)=N(0)\bar{R}^d(0)/[K(Q)t+\bar{R}^3(0)]^{d/3}$.

Comparisons of the present simulations for $g(z)$ and $d=3$, an experimental results [24], and other theories (i.e. MR, ETK, MLSW, Marder) are shown in Fig. 28. The different symbols correspond to distribution function at different times. All these symbols lying on the same line confirm our the YEGG prediction. The present prediction is closer to the simulation and the experimental results.

6. Comparison of Ostwald ripening theories

The theory of Ostwald ripening determines how the second phase particles with time change. Important

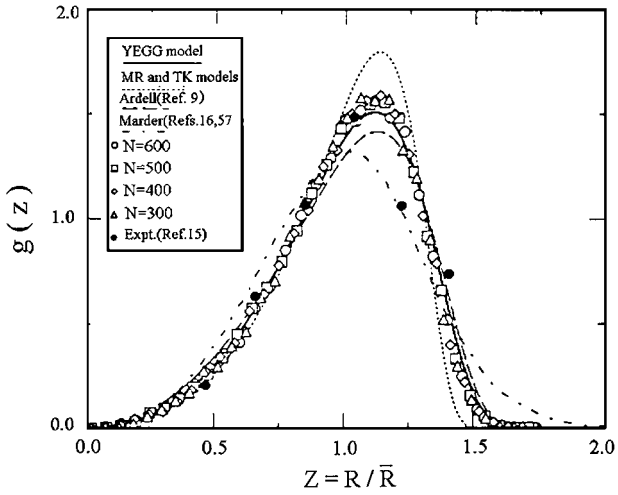

Figure 28 Comparison [15] the distribution functions $g(z)$ with other theories, the simulations and an experiment is displayed in $d = 3$ for $Q = 0.05$. The symbols (except the solid circles) are the simulation results. The different symbols correspond to different times at which the number of remaining particles, $N \cong 600$, 500, 400, and 300. The dotted, long-dahed, dot-dotted, and solid lines are the respective predictions of MR [12], ETK [17], MLSW [8], Marder [16], and YEGG in $d = 3$. Note that the solid circle is the experimental distribution function at very late times [28].

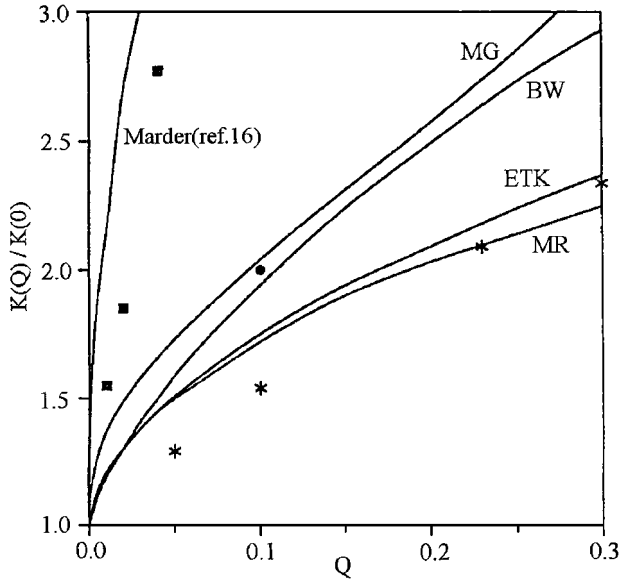

Figure 29 The ratio of $K(Q)/K(0)$ versus the volume fraction Q(19). Also for the comparison the following models are included:Marder [16], BW, TK, ETK (or TK), MR, and Marsh and Glicksman (MG) [59, 60], along with rate constants from the computer simulations of Abinandanan and Johnsson ([61] (■), Beenakker [62] (●), and Voorhees and Glicksman [14] (*).

quantities of interests are the second-phase particle size distribution function $f(R, t)$, the average particle radius $\bar{R}(t)$, and the total number of particles, $N(t)$. The classic Ostwald-ripening theory is attributed to Lifhshitz and Slyzof [5, 6], and Wagner [7] (LSW), who studied the case in which the volume fraction of the second phase tends to zero, i.e., $Q \to 0$, in dimension $d = 3$. This important work revealed both power-law growth and dynamic scaling, which are now considered universal characteristics of the kinetics of a first-order phase transition [55]. Earlier work on extending the theory of LSW to nonzero Q has been attemted by many groups [8–18, 19, 24, 26, 43–46, 56, 57] using both analytic and numerical methods. For the most part, analytic extensions have been based on either on *ad hoc*, (the works of MLSW and TM) or on perturbative expansions in Q, typically taken to order $Q^{1/2}$ [i.e., the works of MR and ETK. In addition, a model was developed by Marder [16] in which two-particle correlations were included for three-dimensional Ostwald ripening.

The important Ostwald ripening theories reviewed in the previous sections, developed to describe systems in which $Q \ll 1$, employed the same microscopic equation to describe the coarsening rates of individual particles, but different procedures to perform the statistical averaging. But, these theories are distinguished on a finer scale [19, 26]. The theories of MR [12], BW [9], and the computer simulations of VG [13, 14] do not account for the effects of interparticle spatial correlations that may develop during ripening, whereas the theories of Marder [16], TK [18], and ETK [18, 58] do consider the influence of these spatial correlations. All of these workers find that the presence of a nonzero volume fraction of coarsening phase does not alter the temporal exponents from those of the theories of LSW, but that it does alter the amplitudes of the power laws. As an example, in his review paper Voorhees [19] has constructed the rate constant plotted as a function of the volume fraction of coarsening phase using the data taken from various works (see Fig. 29). With the exception of Marder's theory, all of the theories mentioned above predict a rather small increase in the rate constant for small volume fractions of coarsening phase and are in close agreement. All of the theories predict that the rate constant will vary as $Q^{1/2}$ in this low volume fraction limit. In addition, all of these theories predict that the scaled time-independent particle radius distributions become broader and more symmetric than those predicted by LSW as the volume fraction increases. Brailsford and Wynblatt (BW) [9], Voorhees and Glickman (VG) [13, 14], Marqusee and Rose (MR) [12], and Tokuyama and Kawasaki (TK) [18], have proposed more realistic models of the coarsening process at finite-volume fractions of coarsening phase.

All these models lead to the following growth law:

$$\bar{R}(t) = [\bar{R}^3(0) + K'(Q)t]^{1/3}$$

where the coarsening rate $K(Q)$ is a monolotically increasing function of Q. The particle-size distribution function satisfies

$$f(R, t) \propto g(z, Q)/\bar{R}^{d+1}$$

where $z \equiv R/\bar{R}$. The theories predict a broadening of $g(z, Q)$ as the volume fraction is increased. Unfortunately, the perturbative theories can neither go beyond $\Theta(\sqrt{Q})$ nor be applied to two-dimensional systems, and the *ad hoc* approaches contain uncontrolled approximations. In many cases, the theories for $d = 3$ give rather different results.

Those Ostwald ripening models which performed the statistical averaging procedure used identical microscopic equations, but they arrived at quantitatively different results [19, 26]. The aim of each of the averaging

procedures employed by BW, VG, TK, and MR is to determine the statistically averaged growth rate $\dot{R}$ or a statistically averaged source/sink strength $B(\dot{R}) = R^2\dot{R}$ of a given particle at a specified Q using Equations 127 and 128. In this averaging procedure, the coarsening phase is again assumed to be spherical and fixed in space. The emission or absorbtion of solute from growing or dissolving particles is modelled by placing point sources or sinks of solute at the center of each particle. Therefore, the diffusion field within the matrix obeys,

$$\Delta^2\theta = +4\pi \sum_{i=1}^{N} B_i \delta(r - r_i) \tag{125}$$

where the source sink strengths B_i are unknowns and $\delta(r - r_i)$ is the Dirac δ function. The solution of Equation 125 is

$$\theta = \theta_m - \sum B_i(r - r_i) \tag{126}$$

where r locates a field point and r_i locates a particle center. The unknown constants B_i and θ_m are determined, as in the LSW treatment, by requiring interfacial equilibrium and solute conservation. The boundary condition along with the solute conversation constraint yields the following set of boundary conditions:

$$B_j = \theta_m R_j - R_j \sum_{\substack{i=1 \\ j=1}}^{N} B_i / B_{ij} \tag{127}$$

$$\theta_m = \theta_o - \alpha \sum_{i=1}^{N} R_i^3 \tag{128}$$

where $R_{ij} \equiv r_j - r_i$. Using Gauss' law and Equation 125 it can shown that $B_i = R_i^2 R_j$.

Using this result that Equation 128 can be reformulated when $t \to \infty$, $\theta_m \to 0$:

$$\sum_{i=1}^{N} B_i = 0 \tag{129}$$

Enomoto *et al.* [17] and Voorhees [26] have summarized each of these statistical averaging source/sink strength $B(\rho)$ procedures, due to various Ostwald ripening models and are given below.

6.1. The Ardell (MLSW) theory

The source/sink strength for this model is

$$B(\rho) = [\xi(Q)\rho - 1][1 + \xi(Q)g_2(Q)\rho] \tag{130}$$

where $\xi(Q)$ is again given by solving Equation 2.19 in [17] and $g_2\,(Q)$ is defined by where $\rho = R/\bar{R}$, $\xi = \bar{R}/R_C$

$$g_2(Q) = 6Q^{1/3} \Big/ \int (x + 8Q)^{-2/3} \exp(-x)\,dx \tag{131}$$

6.2. The BW theory

This model (Section 5.2) employs chemical rate theory to determine the statistically averaged growth rate of a particle, which is the *ad hoc* nature of the rate theory. Brailsford [63] has shown that in the limit of a monodispersion, i.e. diffusion to a random array of absorbing sinks, a statistical average of equations similar to Equation 127 agree with the predictions of the BW effective medium approach.

The predictions of the variation of a particle sink strength with Q derived using the BW effective medium approach in the monodisperse limit are similar to those reported for diffusion-controlled reactions [64]. There are similarities between the MR and BW models. BW use a simple interpolation formula, which yields the following rate equation in the long-time limit,

$$B(\rho) = [\xi(Q)\rho - 1][1 + \xi(Q)g_1(Q)\rho] \tag{132}$$

where $\xi(Q) = \bar{R}/R^*$ and $g_1(Q)$ are given by

$$g_1(Q) = [1/\xi(Q) - 1]/[\xi(Q)m_2(Q) - 1] \tag{133}$$

$$m_3\xi^2 - \{2m_3 + 3Qm_2(m_2 - 1)\}\xi + m_3 + 3Q(m_2 - 1) = 0 \tag{134}$$

$B(\rho)$ is time independent, since $\bar{R}$ and R^* have the same time kinetics as $t \to \infty$. Also, the BW theory reduces to the LSW limit since as $Q \to 0$. Performing a similar asymptotic analysis as LSW, Equation 132 yields the results shown in Figs 30 and 31.

6.3. The MR theory

The MR model (Section 5.5) [12] determine the statistically averaged kinetic equation based on a multiple scattering approach [49, 51]. In this work, the microscopic equation such Equations 127 and 126 are used

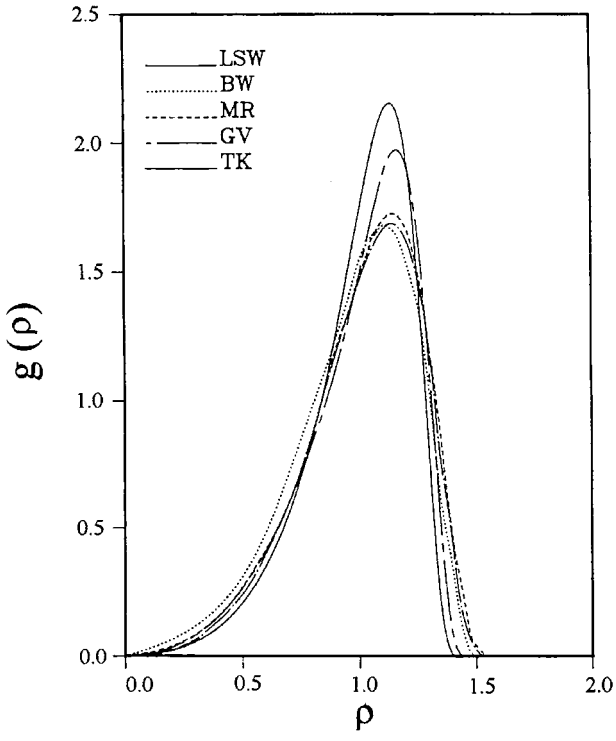

Figure 30 Time-independent scaled particle size distributions versus $\rho = R/\bar{R}$. The distributions due to BW, MR, VG, and TK are all for $Q = 0.1$, and the LSW distribution is for $Q = 0$. [26]

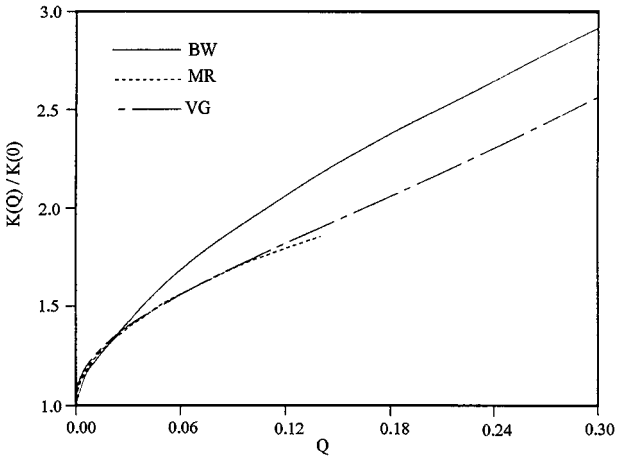

Figure 31 The $K(Q)/K(0)$ ratio versus the volume fraction Q [26].

in the form of an averaged multiple scattering series. In the long-time limit, this theory concludes

$$B(\rho) = (a_o\sigma_1\rho - 1)\left[1 + a_o\rho(3QN_oa_o)^{1/2}\right] \quad (135)$$

Where $\rho = R/\bar{R}$. Here a_o, N_o and σ_1 are the amplitudes of the temporal power laws of the reduced average radius, the number density of particles and the reduced concentration, respectively, in the long time limit, as defined in MR. The rate constants N_o and σ_1 are determined by employing the time independent continuity equation valid in the long time limit and mass conservation. As with TK theory, and $Q \to 0$, $a_o = 1/\sigma_1$ and the LSW distribution and time kinetics are recaptured. $B(\rho)$ is time independent at all volume fractions. Furthermore, for $Q \leq 0.01$ a perturbation treatment predicts that $K(Q) - K(0) \sim Q^{1/2}$. Numerical evaluation of a_o, σ_1, and N_o yields the particle size distribution shown in Fig. 30 along with K(Q) shown in Fig. 31. The MR kinetic equation, at $Q = 0.1$, is also shown in Fig. 32.

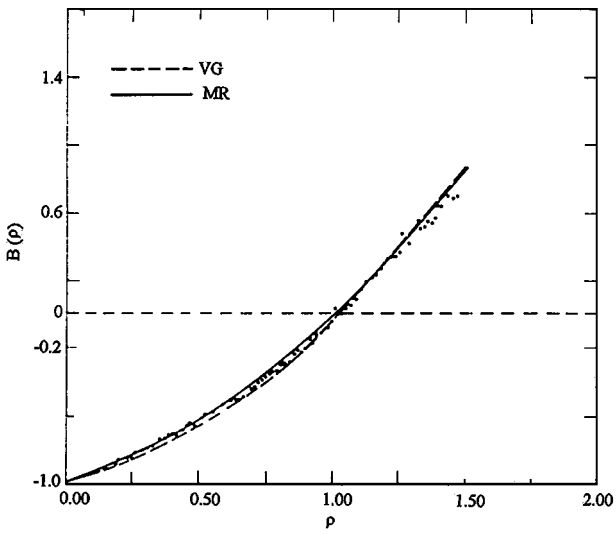

Figure 32 The sink strength $B(\rho) = R^2\dot{R}$ versus ρ at $Q = 0.1$. The nonlinearity of $B(\rho)$ data indicates that diffusional interactions between particles results in an increase in the absolute value of the statistically averaged coarsening rate of a particle [26].

6.4. The TK theory

The TK theory) (Section 5.6) [18] used the statistically averaged Equation 127 through a scaling expansion technique originally developed by Mori and coworkers [73–76]. They find for $\sqrt{3Q} < 1$, in the late stage regime,

$$B(\rho) = \rho - 1 - \rho(M_2 - \rho)(3Q)^{1/2} - C(3Q)^{1/2} \quad (136)$$

where $\rho \equiv R/\bar{R}$, $M_n = \int_0^\infty \rho^n f(R\cdot t)\,dR / \int_0^\infty f(R\cdot t)\,dR$ and C is a complex function of ρ and M_n(25). Their expression for $B(\rho)$ becomes time independent as $t \to \infty$ since $f(R, t) \to g(\rho)h(t)$. As a result, scale-invariant distributions exist in the long-time limit. The first two terms in Equation 136 are simply the LSW kinetic equation in the limit $t \to \infty$ and thus as $Q \to 0$ the TK theory also reproduces the LSW results. The third term is a drift term in particle size space. The fourth term is a soft collision term resulting from the diffusion interactions between particles on distances of order $\sqrt{3Q}/\bar{R}$. In the initial TK paper, they use Equation 136 along with the continuity equation and conclude that the scaled time-independent distributions are a function of Q and that the rate constant K is independent of Q, and find that both K and $g(\rho)$ are functions of Q. The time-independent scaled distribution function found by setting $C = 0$ is shown in Fig. 30.

6.5. The VG theory

Voorhees and Glickman (the VG theory) [13, 14] employ Equations 127 and 129 along with computer simulation techniques to perform the statistical averaging. The periodic nature of the particle arrangement allows Equations 127 to be reformulated into two convergent summations using lattice summation techniques originall developed by Ewald [65]. At finite Q, the coarsening particles interact diffusionally, which results in fluctiations in individual particle coarsening rates. Using the simulations, VG [14] constructed a simple effective medium which reproduces the $B(\rho)$ and rate constant data derived from the simulations over $0.05 \leq Q \leq 0.5$. The VG effective medium approach involves placing a representative particle inside an averaging sphere of radius a, where $a = 1/Q^{1/3}$ for $\rho \leq \rho_C$ and $a = R/Q^{1/3}$ for $\rho \geq \rho_C$, where $\rho = R/\bar{R}$ and $\rho_C = R^*/\bar{R}$. The concentration at the surface of the averaging sphere is a functional of $g(\rho)$, yields the following kinetic equation:

$$B(\rho) = ((\alpha'\rho - 1)(1 + \alpha' Q^{1/3}\rho)S(\rho_c - \rho) + (\alpha'\rho - 1)(1 + Q^{1/3})S(\rho - \rho_c) \quad (137)$$

Where α' is a functional of the moments of $g(\rho)$ and $S(x)$ is a step function defined as 0 for $x < 0$ and 1 for $x > 0$. Clearly as $Q \to 0$ the LSW result is recaptured and $B(\rho)$ is time independent, since α' is only a function of Q. The VG kinetic equation at $Q = 0.1$ is shown in Fig. 32. Asymptotic analysis of the scaled continuity equation and mass conservation constraint yields the results shown in Figs 30 and 31.

6.6. Similarities and dissimilarities in Ostwald ripening theories

In his review work Voorhees [37] has summarized the agreement and disagreement between the various Ostwald ripening theories developed previously (i.e., LSW, BW, VG, MR, TK). Here is this summary:

6.6.1. Similarities in the Ostwald ripening theories

(a) the temporal power laws originally developed by LSW are not a function of Q; however, the amplitude of the power laws is Q dependent; (b) scaled time invarient distribution functions exist at finite Q in the long-time limit; (c) as the particle volume fraction Q increases, the time invarient distributions become broader and more symmetric than the LSW distribution; (d) the rate constant rises rapidly at low Q and is followed by a slower increase with Q; (e) the predictions for $K(Q)$ of VG and MR are almost identical up to $Q \sim 0.1$; and (f) the $B(\rho)$ versus ρ plot in MR and GV are quite similar and in agreement with the VG simulation data, all three descriptions showing increased diffusional interactions with increasing Q which result in an increase in the absolute value of the statistically averaged coarsening rate of a particle in a given size class.

6.6.2. Disagreements in the Ostwald ripening theories

(a) The disagreement between the $K(Q)$ predictions of BW and those of both VG and MR probably originates from BW's use of an *ad hoc* linear interpolation formula; (b) the VG model disagrees with MR for $Q < 10^{-3}$ since MR predict that $K(Q) - K(0) \sim Q^{1/3}$; (c) the TK theory claims that the small difference between the rate constants predicted by TK and MR results from the MR $B(\rho)$ function violating the conservation of mass constraint; (d) The disagreement between the $K(Q)$ prediction of GV, and MR at $Q \geq 0.12$ originates from a breakdown in the assumptions employed by MR; i.e., MR assume that there are no spatial correlations between particles. The simulations performed by VG indicate that spatial correlations begin to occur at $Q \sim 0.1$. Therefore, extension of the MR theory above $Q \sim 0.1$ is probably not justified; (e) the TK model predicts that to order $\sqrt{3Q}$ soft collision terms are present in the $B(\rho)$ function. VG's simulations also suggest that these collision processes should be present and play an important role in the coarsening process. Such collision processes were ignored in the MR model.

7. Concluding remarks: Comparison of Ostwald ripening theories with experiments

An experimental test of the theories describing the effects of a finite volume fraction of corsening phase on the kinetics of Ostwald ripening is difficult problem. The volume fraction of corsening phase must be small and, in particular, the system must satisfy all the assumptions of the theory. The difficulty in producing accurate data is illustrated by the rate constant data in the NiAl system, which have been compiled by Ardell [66]. In this work, for many experiments performed using low volume fractions of Ni_3Al particles in Ni-Al alloy system, the statistical scatter of the data is greater than the factor of 2 or 3 change in the rate constant predicted by some of these theories. Thus it is difficult to conclude on the basis of these data if the volume fraction affects the rate constant in the manner predicted by theory.

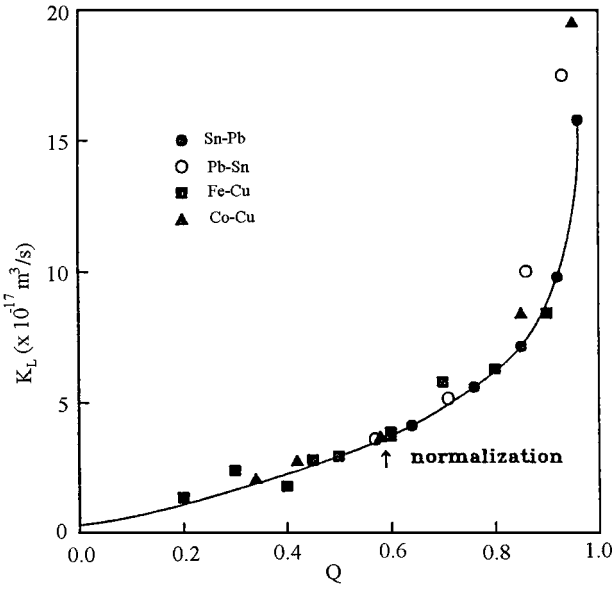

Figure 33 Rate constant [19], K, as a function of volume fraction, Q, following solid-liquid systems: Sn-Pb, Pb-Sn [35], Fe-Cu [69], and Co-Cu [70].

It is clear, however, that the volume fraction of ripening phase does alter the rate constant. Fig. 33 shows a compilation of rate constant data for systems consisting of solid particles in a liquid [67]. In these systems, the ripening rate is quite rapid and a factor of 10 change in the average particle size is easily attainable in most experiments. The line is a cubic spline fit to the data, which employed the rate constant calculated from the LSW theory at $Q = 0$. There is a clear increase in the rate constant with volume fraction and, given the different experimental conditions and alloy systems, it is interesting that all the data appear to fall on one curve.

Mahalingham *et al.* [68] have investigated the Al-Li alloys having different compositions and compared their results with the various Ostwald ripening theories. The theories compared with experiments are the LSW, MLSW, BW, LSEM, TM, VG models. All these theories incorporate the role of volume fraction of the precipitate. It may be useful to briefly summarize the features common to all these theories, so that comparisons of the experimental observations can be made in terms of these features. The main predictions of all the coresening theories are: (a) A steady state distribution of particles develops irrespective of the nature of the assumed initial distribution of particles; (b) a linear relationship between the cube of the average particle size and time, where the slope of this line is the growth rate constant, K; and (c) a broadening of the particle size distribution (PSD) and increase in the

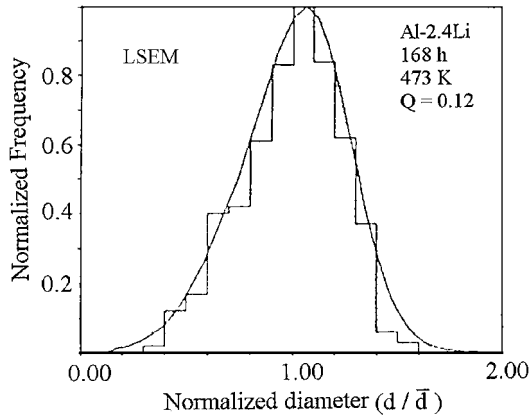

Figure 34 Comparison of the observed particle size distribution for the A1-2.4%Li alloy with the LSEM model [68].

rate constant with an increase in the volume fraction of the precipitate Q.

It appears that only the LSEM theory will be accurate in modelling the particle size distribution even though the other theories also predict a broadening of the distribution with increase in Q. Thus an attempt was made [68] to generate the LSEM distributions corresponding to the volume fractions of δ' phase in Al-Li alloys under investigation. Fig. 34 shows the PSD for Al-2.4% Li alloy. It can be seen that for this alloy the LSEM curve is in rather good agreement with the observed PSD.

In order to compare the observed growth rate constants with those predicted by the Ostwald ripening theories, one needs to evaluate the value of the growth rate constant for the LSW approximation, i.e. at zero volume fraction; $K(0)$. The expression for $K(0)$ is given by

$$K(0) = \frac{8}{9}\frac{C_e \Omega^2 \gamma D}{R_B T} \qquad \text{(see Equation 39)}$$

where Ω is the molar volume of the precipitate (m^3/mol), C_e is the equilibrium solute content of the matrix (mol/m^3), γ is the surface energy (J/m^2) and D is the diffusion coefficient (m^2/s). The calculated values were in closer agreement to the values predicted by MLSW theory and were significantly greater than those predicted by the other theories. The ratios $K(Q)/K(0.12)$ was computed and compared with the corresponding ratios predicted by the theories. The results [68] are shown in Table I. Again, the experimentally determined ratio was in closer agreement to the MLSW theory than the other models.

Alternatively, we may compute the values of $K(0)$ each theory, as determined from the predicted value of $K(Q)/K(0)$ and the experimental value of $K(Q)$. Using this value $K(0)$, the $K(Q)/K(0)$ for other values of $K(Q)$ can be computed and this can be compared with the predicted values. Thus the value of $K(0)$ was calculated from $K(0.12)/K(0)$ and the results have been tabulated [68] in Table II. Here again, it is seen that MLSW values are more in agreement with the observed values.

TABLE I Comparison of the observed and theoretically predicted $K(Q)/K(0)$, for $K(Q)$ [68]

	$\frac{K(Q)}{K(0.12)}$	$\frac{K(Q)}{K(0.12)}$	$\frac{K(Q)}{K(0.12)}$	$\frac{K(Q)}{K(0.12)}$	$\frac{K(Q)}{K(0.12)}$
Q	Measured	MLSW	BW	LSEM	VG
0.12	1	1	1	1	1
0.24	1.67	1.56	1.32	1.14	1.29
0.26	2.08	1.78	1.38	1.17	1.33
0.45	2.39	2.56	1.82	1.34	2.14
0.55	3.44	3.13	1.89	1.44	2.5

The above calculations indicate that all the theories mentioned above except the MLSW theory, underestimate the effect of volume fraction on the growth rate constant. It was suggested [68] that this could be due to the contribution of particle encounters in increasing the growth rate of particles, which might be fortuitous. In spite of its good agreement with the observed PSD_s, the LSEM model predicts very low rate constants. As pointed out by Voorhees and Glickman [14], this could be due to the assumption in the LSEM model, that the LSW growth rate equation is valid for nonzero volume fractions.

Calderon and Fine [71] have studied the corsening kinetics of NiAl type precipitate particles in Fe-Ni-Al-Mo alloys. They have investigated the effects of the volume fraction Q of precipitates and compared the experimental results with the theoretical predictions of the LSW and BW models. They calculated the $K(4.4)/K(0)$ ratio to be 1.61 for the BW model. Using Equation 39 and the $K(4.4)/K(0)$ ratio the value of the interfacial energy γ was evaluated as 1.8–2.6 $\times 10^{-2}$ Jm^{-2}. The VG model [72] predicts the 1.4 and 1.27 values for the $K(6.4)/K(0)$ and $K(4.4)/K(0)$ ratios, respectively. From this ratios the interfacial energy was calculated [71] to be (2.3–3.3) $\times 10^{-2}$ Jm^{-2} in the same alloy. The slight differences with the predictions of the BW model do not appreciably change the value of γ, if the experimental error is taken into account. Fig. 35 shows

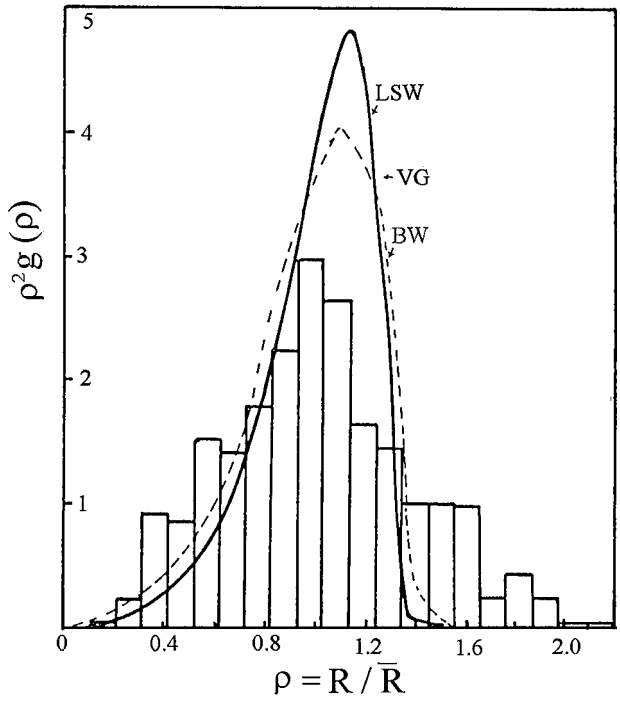

Figure 35 Particle size distributions for the aging time 100 h at 700°C in Fe-Ni-Al-Mo alloy. For the comparison the works of LSW and BW are also included [71].

TABLE II Comparison of observed and theoretically predicted $K(Q)/K(0)$ ratios for $K(Q)$ [68]

Q	MLSW		BW		LSEM		VG	
	$\left[\frac{K(Q)}{K(0)}\right]_p$	$\left[\frac{K(Q)}{K(0)}\right]_o$	$\left[\frac{K(Q)}{K(0)}\right]_p$	$\left[\frac{K(Q)}{K(0)}\right]_o$	$\left[\frac{K(Q)}{K(0)}\right]_p$	$\left[\frac{K(Q)}{K(0)}\right]_o$	$\left[\frac{K(Q)}{K(0)}\right]_p$	$\left[\frac{K(Q)}{K(0)}\right]_o$
0.12	6.15	6.15	2.07	2.07	1.36	1.36	1.7	1.7
0.24	9.61	10.27	2.73	3.46	1.56	2.27	2.20	2.84
0.26	10.96	12.78	2.37	4.30	1.6	2.83	2.25	3.54
0.45	15.76	14.72	3.78	4.96	1.83	3.26	3.64	4.07
0.55	19.23	21.16	3.91	7.12	1.96	4.68	4.25	5.85

$[K(Q)/K(0)]_p$: Predicted ratio; $[K(Q)/K(0)]_o$: Observed ratio.

TABLE III Moments of the theoretical and experimental particle size distributions for $Q = 4.4$ for an Fe-Ni-Al-Mo alloy aged at different times [71]

Size distribution	Variance	Skewness	Kurtosis
Alloy; 5 h	0.099	1.5217	5.7073
Alloy; 30 h	0.0716	0.2905	3.6126
Alloy; 50 h	0.0873	2.2097×10^{-3}	3.4991
Alloy; 100 h	0.1398	0.2711	2.7083
BW ($Q = 4.4$) [9]	0.056525	−0.71638	3.1915
TM ($Q = 4.0$, model III [11]	0.06127	−0.67786	3.11233
TM ($Q = 4.0$, model III [11]	0.08214	−0.46551	2.73655
(LESM) ($Q = 4.4$) [10]	0.05948	−0.4987	3.188

the particle size distributions determined from precipitate measurements. In this figure the ordinates $\rho^2 h(\rho)$ where ρ represents the normalized particle size as defined by the LSW. Empirically $\rho^2 h(\rho)$ was calculated [30] according to

$$\rho^2 h(\rho) = \frac{N(R, R + \Delta R)}{\sum(R, R + \Delta R)} \cdot \frac{\bar{R}}{\Delta R} \cdot \frac{9}{4}$$

The distribution function predicted by the LSW and BW models have been superimposed on the empirical histograms in Fig. 35.

Table III shows a quantitative comparison between the empirical and theoretical distributions which is based on the calculation of the moments of the size distribution as well as the coefficients skewness and kurtosis. Table III also shows the results predicted by the BW, TM (two of the six models developed by the TM) and LSEM models. In all these cases, poor agreement was found especially in the skewness parameter where a negative value is invariably predicted and the the empirical result yields either a positive or at least a considerably less negative value. The quantitative comparison suggests that volume fraction effects are not the only effects that need to be taken into consideration in the Ostwald ripenin theory. Other effects such as the interactions of dislocations were suggested [71] to give rise to the accelarated growth of some particles (as a result of fast diffusion).

Although the aforementioned theories are by far the most realistic theories of Ostwald ripening yet developed, they are only in qualitative agreement on the role of finite volume fractions on the coarsening behaviour of two-phase systems. Unfortunately, a crucial experiment has not been performed at low Q in order to compare to the theories. Work at higher Q is in qualitative agreement with the aformentioned theoretical predictions, i.e., time-independent distribution functions which are broader and more symmetric than LSW.

According to our knowledge, a coarsening experiment has never been done using a system for which all the relavent materials parameters were known priori. Such an approach would permit a direct measurement of $K(Q)$. Clearly more experimental and theoretical work is necessary in order to settle the subtle disagreement now existing between the various Ostwald ripening theories.

References

1. W. OSTWALD, *Z. Phys. Chem.* **37** (1901) 385.
2. *Idem.*, "Analytisch Chemie," 3rd ed. (Engelmann, Leipzig, 1901).
3. G. W. GREENWOOD, *Acta Met.* **4** (1956) 243.
4. R. ASIMOV, *ibid.* **11** (1962) 72.
5. I. M. LIFSHITZ and V. V. SLYOZOV, *J. Phys. Chem. Solids* **19** (1961) 35.
6. *Idem.*, *Sov. Phys.: Solid State* **1** (1960) 1285.
7. C. WAGNER, *Z. Electrochem.* **65** (1961) 581.
8. A. J. ARDELL, *Acta Met.* **20** (1972) 61.
9. A. D. BRAILSFORD and P. WYNBLATT, *ibid.* **27** (1979) 489.
10. C. K. L. DAVIES, P. NASH and R. N. STEVENS, *ibid.* **28** (1980) 179.
11. K. TSUMARAYA and Y. MIYATA, *ibid.* **31** (1983) 437.
12. J. A. MARQUSEE and J. ROSE, *J. Chem. Phys.* **80** (1984) 536.
13. P. W. VOORHEES and M. E. GLICKSMAN, *Acta Met.* **32** (1984) 2001.
14. *Idem.*, *ibid.* **32** (1984) 2013.
15. J. H. YAO, K. R. ELDER, H. GUO and M. GRANT, *Phys. Review* B **47** (1993) 14100.
16. M. MARDER, *Phys. Review* A **36** (1987) 858.
17. Y. ENOMOTO, M. TOKUYAMA and K. KAWASAKI, *Acta Met.* **34** (1986) 2119.
18. M. TOKUYAMA and K. KAWASAKI, *Physica* A **123** (1984) 386.
19. P. W. VOORHEES, *Annu. Rev. Mater. Sci.* **22** (1992) 197.
20. S. CORIELL and R. L. PARKER, *J. Appl. Phys.* **36** (1965) 632.
21. J. W. GIBBS, 1906, "The Collected Works of J. W. Gibbs" (Longmans, Green and Co, Dover, New York).
22. M. HILLERT, "Lectures on the Theory of Phase Transformations" (New York, 1975).
23. P. W. VOORHEES, Ph.D. Thesis, Rensselaer Polytechnique Institue, 1982.
24. P. W. VOORHEES and M. E. GLICKSMAN, *Metall. Trans.* A **15A** (1984) 1081.
25. J. J. WEIN and J. W. CAHN, "Sintering and Related Phenomena" (Plenum Press, London, 1973) p. 151.
26. P. W. VOORHEES, *J. Statistical Physics* **38** (1985) 231.
27. R. D. VENGRENOVITCH, *Acta Met.* **30** (1982) 1079.
28. P. K. RASTOGI and A. J. ARDELL, *Acta Met.* **19** (1971) 321.
29. D. H. JACK and R. W. K. HONEYCOMBE, *Acta Met.* **20** (1972) 787.
30. A. J. ARDELL and R. B. NICHOLSON, *J. Phys. Chem. Solids* **27** (1966) 1793.

31. M. CHATURVEDI and D. W. CHUNG, *J. Inst. Metals* **101** (1973) 253.
32. D. J. CHELLMAN and A. J. ARDELL, *Acta Met.* **22** (1974) 577.
33. Y. SENO, Y. TOMOKIYO, K. OKI and T. EZUCHI, *Trans. Japan Inst. Metals* **24** (1983) 491.
34. T. HIRATA and D. H. KIRKWOOD, *Acta Met.* **25** (1977) 1425.
35. S. C. HARDY and P. W. VOORHEES, *Metall. Trans.* A **19** (1988) 2713.
36. A. J. ARDELL, "The Mechanism of Phase Transformations in Crystalline Solids" (Institute of Metals, London, 1969) p. 111.
37. M. HILLERT, "Lectures on the Theory of Phase Transformations" (Am. Inst. Min. Pet. Metall. Eng, New York, 1975).
38. N. BOWER and J. A. WHITEMAN, "The Mechanism of Phase Transformations in Crystalline Solids" (Inst. of Metals, London, 1969) p. 119.
39. P. WIRTZ and M. E. FINE, *J. Amer. Ceramic Soc.* **51** (1968) 402.
40. T. HIRATA and D. H. KIRKWOOD, *Acta Met.* **25** (1977) 1425.
41. C. H. KANG and D. N. YON, *Met. Trans.* A **12A** (1981) 65.
42. Y. MASUDA and R. WATANABE, in "Sintering Processes," Materials Science Research, Vol. 13, edited by G. C. Kuczynski (Plenum, New York, 1979) p. 3.
43. M. TOKUYAMA, K. KAWASAKI and Y. ENOMOTO, *Physica* **134A** (1986) 323.
44. K. KAWASAKI, Y. ENOMOTO and M. TOKUYAMA, *ibid.* **135A** (1986) 426.
45. C. W. BEENEKKER, *Phys. Rev.* A **33** (1986) 4482.
46. A. J. ARDELL, *Phys. Rev.* B **41** (1990) 2554.
47. B. U. FELDERHOF and J. M. DEUTCH, *J. Chem. Phys.* **64** (1976) 4551.
48. M. MUTHUKUMAR and R. I. CUKIER, *J. Stat. Mech.* **26** (1981) 453.
49. M. BIXON and R. ZWANZIG, *J. Chem. Phys.* **75** (1981) 2359.
50. T. R. KIRKPATRICK, *ibid.* **76** (1982) 4255.
51. M. TOKUYAMA and R. I. CUKIER, *ibid.* **76** (1982) 6202.
52. J. A. MARQUSEE and J. ROSS, *ibid.* **79** (1983) 373.
53. H. WENDT and P. HANSEN, *Acta Met.* **31** (1983) 1649.
54. M. E. GLICKSMAN and P. VOORHEES, "Phase Transformations in Solids" (edited by Tsakalakos) p. 451.
55. J. D. GUNTON, M. SAN MIGUEL and P. S. SAHNI, in "Phase Transformations and Critical Phenomena," Vol. 8, edited by C. Domb and J. L. Lebowitz (Academic, London, 1983).
56. M. MARDER, *Phys. Rev. Lett.* **55** (1985) 2953.
57. J. H. YAO, K. R. ELDER, H. GUO and M. GRANT, *Phys. Rev.* B **45** (1992) 8173.
58. Y. ENOMOTO, M. TOKUYAMA and K. KAWASAKI, *Acta Met.* **35** (1987) 907.
59. S. P. MARSH, Ph.D. thesis, 1991, Rensselaer Polytechniques Institute.
60. *Idem.*, In "Simulation and Theory of Evolving Microstructures," edited by M. P. Anderson and A. D. Rollet (Warrendale, Penn. Min. Mater. Soc.) p. 167.
61. W. C. JOHNSON, T. A. ABINANDANAN and P. W. VOORHEES, *Acta Metall.* **38** (1990) 1349.
62. C. W. J. BEENAKKER, *Phys. Rev.* A **33** (1986) 4482.
63. A. D. BRAILSFORD, *J. Nuc. Mater.* **60** (1976) 257.
64. D. F. CALET and J. M. DEUTCH, *Ann. Rev. Phys. Chem.* **34** (1983) 394.
65. P. P. EWALD, *Ann. Phys. (Leipzig)* **64** (1921) 253.
66. A. J. ARDELL, *Scripta Met.* **24** (1990) 343.
67. S. C. HARDY, N. AKAIWA and P. W. VOORHEES, *Acta Met.* **39** (1991) 2931.
68. K. MAHALINGAM, B. P. GU and G. L. LIEDL, *ibid.* **35** (1987) 483.
69. A. N. NIEMI and T. H. COURTNEY, *Acta Met.* **3** (1981) 1393.
70. C. H. KANG and D. N. YOON, *Metall. Trans.* A **12** (1981) 65.
71. H. CALDERON and M. E. FINE, *Mater. Sci. And Eng.* **63** (1984) 197.
72. N. BOWER and J. A. WHITEMAN, "The Mechanism of Phase Transformations in Crystalline Solids" (Inst. of Metals, London, 1969) p. 119.

Received 5 March 2000
and accepted 19 December 2001